BIOE 476: Tissue Engineering, Fall 2018

Take-Home Questions/In-class Discussion, October 25th

Part 1

Consider these questions related to the article: Engler et al. Matrix elasticity directs stem cell lineage specification. Cell (2006) vol. 126 (4) pp. 677-89.

1. Typically, increasing the ECM density will result in increased stiffness as well as increased density of ECM ligands (which results in increased signaling). In this paper, how do the authors decouple ECM stiffness from ECM ligand density, in order to focus only on the effects of mechanical stiffness?

2. The addition of Blebbistatin is used as a condition in many of the experiments in the paper. What is the function of Blebbistatin? What is its role in these experiments and what is revealed by the experimental data?

3. What effect do stiffer substrates have on focal adhesions? What effect do stiffer substrates have on actin assembly?

4. The last paragraph of the paper (prior to experimental procedures) discusses the implications of these research findings as related to stem cell therapy in the heart. In your own interpretation/words, what is the concern that the authors are trying to raise?

5. Can you think of any differences between the experimental system in this paper and normal in vivo environments that may affect the interpretation?

Part 2

Read this recent follow-up article: Wen et al. Interplay of matrix stiffness and protein tethering in stem cell differentiation. Nat Mat (2014), 13, 979-987.

http://www.nature.com/nmat/journal/v13/n10/full/nmat4051.html

6. For the polyacrylamide-based approach, the authors perform experiments to rule out an alternative explanation for their 2006 findings that implicated material stiffness in guiding stem cell differentiation. What is this alternative explanation and what did they test to rule it out?

Cell

Matrix Elasticity Directs Stem Cell Lineage Specification

Adam J. Engler,[1,2] Shamik Sen,[1,2] H. Lee Sweeney,[1] and Dennis E. Discher[1,2,3,4,*]
[1] Pennsylvania Muscle Institute
[2] School of Engineering and Applied Science
[3] Cell & Molecular Biology Graduate Group
[4] Physics Graduate Group
University of Pennsylvania, Philadelphia, PA 19104, USA
*Contact: discher@seas.upenn.edu
DOI 10.1016/j.cell.2006.06.044

SUMMARY

Microenvironments appear important in stem cell lineage specification but can be difficult to adequately characterize or control with soft tissues. Naive mesenchymal stem cells (MSCs) are shown here to specify lineage and commit to phenotypes with extreme sensitivity to tissue-level elasticity. Soft matrices that mimic brain are neurogenic, stiffer matrices that mimic muscle are myogenic, and comparatively rigid matrices that mimic collagenous bone prove osteogenic. During the initial week in culture, reprogramming of these lineages is possible with addition of soluble induction factors, but after several weeks in culture, the cells commit to the lineage specified by matrix elasticity, consistent with the elasticity-insensitive commitment of differentiated cell types. Inhibition of nonmuscle myosin II blocks all elasticity-directed lineage specification–without strongly perturbing many other aspects of cell function and shape. The results have significant implications for understanding physical effects of the in vivo microenvironment and also for therapeutic uses of stem cells.

INTRODUCTION

Adult stem cells, as part of normal regenerative processes, are believed to egress and circulate away from their niche (Katayama et al., 2006), and then engraft and differentiate within a range of tissue microenvironments. The tissue or matrix microenvironments can be as physically diverse as those of brain, muscle, and bone precursor osteoid (respectively, Flanagan et al. 2002; Georges et al., 2006; Kondo et al., 2005, Engler et al., 2004a; Ferrari et al., 1998; Andrades et al., 2001; Holmbeck et al., 1999; Morinobu et al., 2003). Mesenchymal stem cells (MSCs) are marrow-derived and have indeed been reported to differentiate into various anchorage-dependent cell types, including neurons, myoblasts, and osteoblasts (respectively, [Deng et al., 2005; Hofstetter et al., 2002; Kondo et al., 2005], [Pittenger et al., 1999], and [McBeath et al., 2004; Pittenger et al., 1999]). For differentiated cells such as fibroblasts, it is well known that responses to the typical soluble inducers such as growth factors couple to matrix anchorage (Nakagawa et al., 1989). However, with naive stem cells, direct effects of matrix physical attributes such as matrix stiffness have yet to be examined.

Differentiated cells ranging from neurons to osteoblasts adhere, contract, and crawl not only within soft tissues such as that of the brain or on top of crosslinked collagen ''osteoids'' in remodeling bone but also in vitro on collagen-coated acrylamide gels and glass (Figure 1A). Such a wide variation in matrix stiffness for differentiated cells is known to influence focal-adhesion structure and the cytoskeleton (Bershadsky et al., 2003; Cukierman et al., 2001; Discher et al., 2005; Engler et al., 2004a; Lo et al., 2000; Pelham and Wang, 1997). Past results with cells committed to a particular lineage, especially fibroblasts, on floating collagen gels and wrinkling-silicone sheets also suggest some responsiveness to the physical state of the matrix (Hinz et al., 2001; Nakagawa et al., 1989; Tomasek et al., 2002; Wozniak et al., 2003), but gel porosity and film topography complicate identification of possible contributions of substrate stiffness. In contrast, tissue-level matrix stiffness is distinct and shown here in sparse cultures to exert very strong effects on the lineage specification and commitment of naive MSCs, as evident in cell morphology, transcript profiles, marker proteins, and the stability of responses.

How might MSCs ''feel'' or sense matrix elasticity and transduce that information into morphological changes and lineage specification? At the molecular scale, matrix sensing first requires the ability to pull against the matrix and, secondly, requires a cellular mechano-transducer(s) to generate signals based on the force that the cell must generate to deform the matrix. Of the cell's cytoskeletal motors, one or all of the nonmuscle myosin II isoforms (NMM IIA, B, and C [Kim et al., 2005]) are candidates, as they are implicated in tensioning cortical actin structures

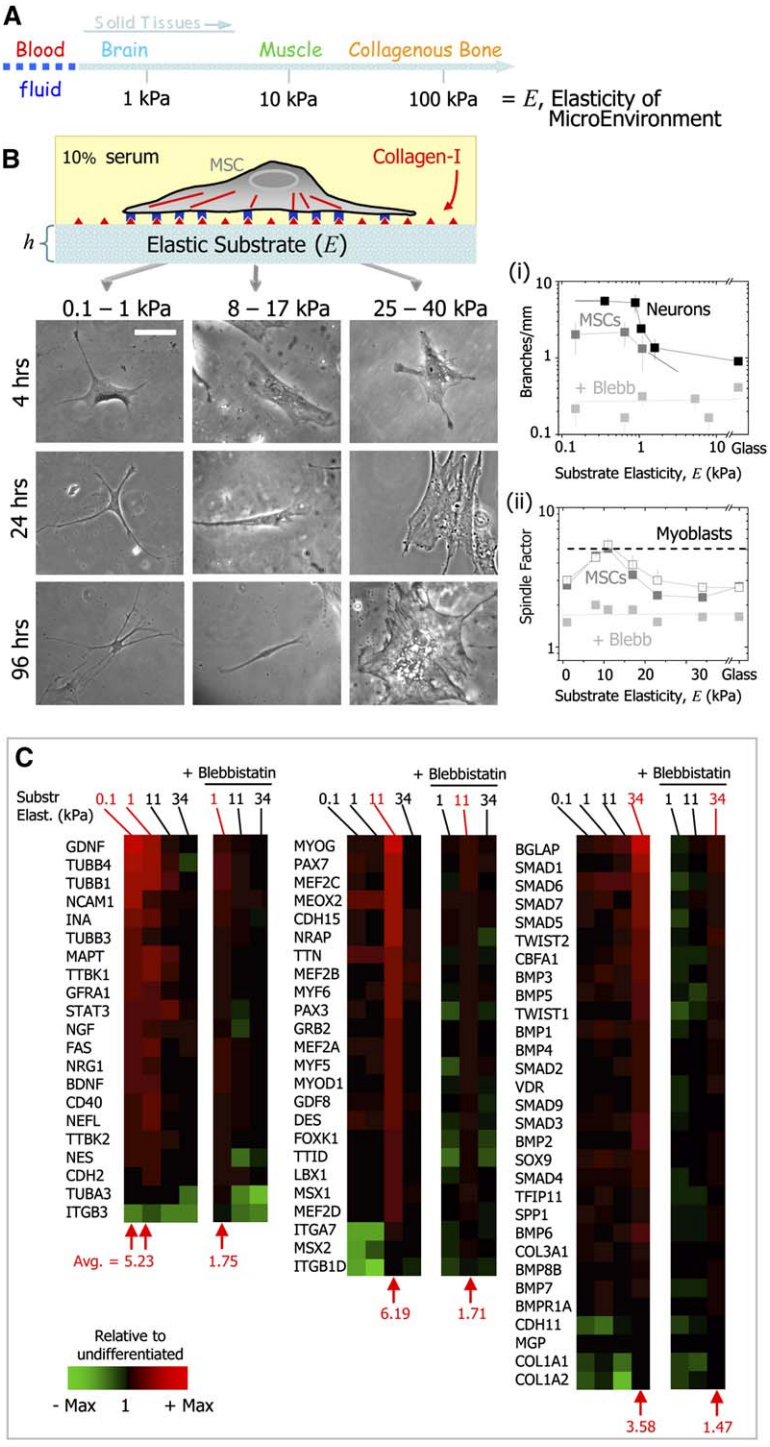

Figure 1. Tissue Elasticity and Differentiation of Naive MSCs

(A) Solid tissues exhibit a range of stiffness, as measured by the elastic modulus, *E*.

(B) The in vitro gel system allows for control of *E* through crosslinking, control of cell adhesion by covalent attachment of collagen-I, and control of thickness, *h*. Naive MSCs of a standard expression phenotype (Table S1) are initially small and round but develop increasingly branched, spindle, or polygonal shapes when grown on matrices respectively in the range typical of $\sim E_{brain}$ (0.1–1 kPa), $\sim E_{muscle}$ (8–17 kPa), or stiff crosslinked-collagen matrices (25–40 kPa). Scale bar is 20 μm. Inset graphs quantify the morphological changes (mean ± SEM) versus stiffness, *E*: shown are (*i*) cell branching per length of primary mouse neurons (Flanagan et al., 2002), MSCs, and blebbistatin-treated MSCs and (*ii*) spindle morphology of MSCs, blebbistatin-treated MSCs, and mitomycin-C treated MSCs (open squares) compared to C2C12 myoblasts (dashed line) (Engler et al., 2004a).

(C) Microarray profiling of MSC transcripts in cells cultured on 0.1, 1, 11, or 34 kPa matrices with or without blebbistatin treatment. Results are normalized to actin levels and then normalized again to expression in naive MSCs, yielding the fold increase at the bottom of each array. Neurogenic markers (left) are clearly highest on 0.1–1 kPa gels, while myogenic markers (center) are highest on 11 kPa gels and osteogenic markers (right) are highest on 34 kPa gels. Blebbistatin blocks such specification (<2-fold different from naive MSCs).

(McBeath et al., 2004; Wang et al., 2002). These actin structures are in turn linked to focal adhesions that provide the pathway of force transmission from inside the cell to the elastic matrix (Beningo et al., 2001; Tamada et al., 2004) and associated with the focal-adhesion complexes are a number of well-known signaling molecules that are well-placed to act as the mechano-transducers (Bershadsky et al., 2003; Alenghat and Ingber, 2002). With MSCs here, we demonstrate that one or all of the NMM IIA–C are likely to be involved in the matrix-elasticity sensing that drives lineage specification.

The resistance that a cell feels when it deforms the ECM is measured by the elastic constant, *E*, of the matrix or microenvironment. For microenvironments of relevance here,

that of the brain (Flanagan et al., 2002) is considerably softer than muscle (Engler et al., 2004a), and muscle is softer than collagenous osteoid precursors of bone (measured here). The wide range of microenvironment elasticity highlighted in Figure 1A is central, we show, to predicting specification of MSCs. Matrix elasticity is mimicked in vitro here with inert polyacrylamide gels in which the concentration of bis-acrylamide crosslinking sets the elasticity (Pelham and Wang, 1997), and adhesion is provided by coating the gels with collagen I, which is known to support myogenic and osteogenic differentiation (Engler et al., 2004a; Garcia and Reyes, 2005). Using this well-defined, elastically tunable gel system (Figure 1B), as opposed to wrinkling films or degrading collagen gels (Hinz et al., 2001; Wozniak et al., 2003), we provide the first evidence with sparse cultures of MSCs that matrix can specify lineage toward neurons, myoblasts, and osteoblasts—all in identical serum conditions. We document the matrix regulation of key lineage markers and myosins, including NMM IIs, which—when inhibited with blebbistatin (Straight et al., 2003)—blocks differentiation. We also show that soluble induction factors tend to be less selective than matrix stiffness in driving specification, and cannot reprogram MSCs that are precommitted for weeks on a given matrix. Finally, by controlling gel thickness, h, we establish how far stem cells can feel and thus physically define their microenvironment.

RESULTS

Cell Morphology Suggests Lineage Specification Is Directed by Matrix Stiffness and Dependent on Nonmuscle Myosin II

On soft, collagen-coated gels that mimic brain elasticity ($E_{brain} \sim 0.1$–1 kPa) (Flanagan et al., 2002), the vast majority of MSCs adhere, spread, and exhibit an increasingly branched, filopodia-rich morphology (Figure 1B). Branching densities after 1 week in culture approach those of primary neurons on matrigel-coated gels (Flanagan et al., 2002), and the dynamics of outward extension with branching is clearly opposite to DMSO-induced retraction of the cell body that can leave pseudoextensions behind (Neuhuber et al., 2004). MSCs on 10-fold stiffer matrices that mimic striated muscle elasticity ($E_{muscle} \sim 8$–17 kPa) lead to spindle-shaped cells similar in shape to C2C12 myoblasts (Engler et al., 2004a). Stiffer matrices (25–40 kPa) that we show below mimic the crosslinked collagen of osteoids (Garcia and Reyes, 2005; Kong et al., 2005) yield polygonal MSCs similar in morphology to osteoblasts. Analyses of cell morphologies (Figure 1B; plots i and ii) show that matrix-dependent shape variations of MSCs are similar to differentiated cells. It is important to also note in these plots and elsewhere below that the results with stiff acrylamide gels extrapolate to those with collagen-coated, rigid glass; this is expected if substrate elasticity is a key variable of importance. Furthermore, since the inhibition of proliferation by mitomycin-C (open squares, Figure 1B; plot ii) has little impact on average cell shape, the morphology results are consistent with lineage development being a population-level response to substrate elasticity.

As introduced above, nonmuscle myosin II is likely to be involved in exerting force through focal adhesions in mechanisms of sensing matrix elasticity. All of the NMM II isoforms are inhibited by blebbistatin, which does not inhibit any other myosin found in MSCs (see below), other than myosin VI (Limouze et al., 2004). Addition of blebbistatin during plating blocks branching, elongation, and spreading of MSCs on any substrate (Figure 1B; plots); however, addition of blebbistatin 24 hr postplating does not significantly reverse cell shape or spreading on E_{muscle} gels after the cells have already spread and adopted a spindle morphology (e.g., 24 hr per Figure 1B). Less specific and less potent myosin inhibitors such as BDM (at ~mM concentrations) are already known to block neuronal motility as well as the sensitivity of differentiated cells to substrate elasticity (Pelham and Wang, 1997), but blebbistatin is far more selective and potent (Straight et al., 2003). It inhibits actin activation of NMM II ATPase activity (at ~μM concentrations) and blocks migration and cytokinesis in vertebrate cells without affecting MLCK. Crystal structures show inhibition of actin-activated ATPase activity by blebbistatin (Allingham et al., 2005) requires a specific alanine (or serine) residue that is found only in class II and VI myosins (Limouze et al., 2004; Straight et al., 2003). We confirm below that MSCs express the three NMM IIs and myosin VI, but we implicate NMM IIs and the cytoskeleton as critical to differentiation.

To reinforce this conclusion and to rule out a role for myosin VI in matrix sensing, we repeated the above experiments with the myosin light chain kinase (MLCK) inhibitor, ML7 (Dhawan and Helfman, 2004). Of the myosins found in MSCs thusfar (see below), regulatory light chain phosphorylation via MLCK is only used to activate the NMM IIs. ML7 will block activation of these as well as smooth muscle myosin isoforms but will not affect activation of any other myosins in MSCs. Results with ML7 prove below to be identical to those seen with blebbistatin, and so NMM II activity appears to be necessary for matrix elasticity-driven lineage specification.

RNA Profiles Indicate Lineage Specification on Matrices of Tissue-like Stiffness

Transcriptional profiles of neurogenic, myogenic, and osteogenic markers—from early commitment markers through mid/late development markers—prove consistent with indications from morphology. On the softest gels, MSCs show the greatest expression of neurogenic transcripts (Figure 1C, left column; Table S3). Neuron-specific cytoskeletal markers such as nestin, an early commitment marker, and β3 tubulin, expressed in immature neurons, as well as the mature marker neurofilament light chain (NFL) (Lariviere and Julien, 2004) and the early/midadhesion protein NCAM (Rutishauser, 1984), are all upregulated. In terms of a simple average across various key

neurogenic transcripts, upregulation on the softest gels is 5-fold above early passage MSCs. On moderately stiff matrices near E_{muscle} (11 kPa), MSCs express 6-fold more myogenic message, with clear upregulation of early to late transcriptional proteins such as Pax activators and myogenic factors (e.g., MyoD); comparisons of expression levels to committed muscle cells are also provided below. On the stiffest matrices (34 kPa), MSCs express 4-fold greater osteogenic message, upregulating osteocalcin and the early transcriptional factor CBFα1 (middle and right column, respectively). Importantly, transcriptional profiles of early versus late MSCs (up to passage 12) do not differ significantly (Table S1), even though population expansion has been suggested by others to dramatically alter MSCs (Maitra et al., 2005). However, lineage specification on each matrix is clearly blebbistatin sensitive (Figure 1C + blebbistatin).

A number of terminal differentiation markers such as lineage specific integrins (α3, α7, and β1D) and morphogenetic proteins are not upregulated relative to naive MSCs. However, these are generally not expressed until later development, e.g., cell fusion into myotubes is required for β1D expression. Matrix stiffness undoubtedly couples to cell density for fusion and synaptogenesis as well as other noncollagenous ECM components and soluble factors (see below).

Clarifying Neuro-Induction and Osteogenic Microenvironments

The results above and that follow below provide insight into the NMM II-based contractility and considerable sensitivity of stem cells to mechanical microenvironment, which are important issues in and of themselves, but the results also bring to the fore several questions in the literature regarding induction strategies and the physical nature of in vivo microenvironments. For example, uncertainty exists regarding the inducibility of stem cells toward neurogenic lineages. Soluble agonists such as retinoic acid and dimethylsulfoxide (DMSO) have been reported to induce reversible branching in stem cells (Dinsmore et al., 1996; Woodbury et al., 2002), but DMSO also causes fibroblasts to appear "branched," and this appears due to cytoskeletal disruption with centripetal retraction of the cell body that leaves extensions attached (Neuhuber et al., 2004).

The time series of images in Figure 1B shows outwardly branching MSCs on the softest gels (0.1–1 kPa) which, in immunofluorescence (Figure 2A), also show expression and branch localization of neuron-specific β3 tubulin and neurofilament heavy chain (NFH and its phosphoform, P-NFH). The latter are widely recognized as late neuronal markers (Lariviere and Julien, 2004). Indeed, both MSCs and primary neurons (Flanagan et al., 2002) spread and branch with time on the softest matrices (Figure 2B), unlike fibroblasts that do not branch or express neurogenic proteins. Similarly, on myogenic matrices, both MSCs and myoblasts spread and become spindle shaped with time, unlike fibroblasts (Figure S1A). Intensity analyses of immunofluorescent images (e.g., Figures 2A and 2C) as well as Western blots (Figure 2C; inset) confirm that only cells on the softest matrices express protein markers for neuronal commitment (nestin), immature neurons (β3 tubulin), mid/late neurons (microtubule associated protein 2; MAP2), and even mature neurons (NFL, NFH, and P-NFH). These findings clearly agree with neurogenesis of MSCs, as seen in more complex microenvironments, especially the brain (Kondo et al., 2005; Wislet-Gendebien et al., 2005).

Uncertainty also exists in the literature regarding the compliance and thickness of osteoid. This crosslinked collagen precursor to bone is secreted by osteoblasts and reportedly is the matrix upon which MSCs undergo a transition to preosteoblasts (Figure 2D) (Andrades et al., 2001; Morinobu et al., 2003; Raisz, 1999), before the matrix calcifies over week(s) (Rattner et al., 2000) to rigid bone ($\sim 10^6$ kPa). We have made the first measurements here of the compliance and thickness of the osteocalcin-rich osteoid matrix (Figure 2E) that surrounds osteoblasts in culture (see AFM in Experimental Procedures). The matrix is 350 $\pm$ 100 nm thick (Figure 2F) and has a stiffness, $E_{osteoid} \sim 27 \pm 10$ kPa (Figure 2G), that is similar to a concentrated collagen gel (Roeder et al., 2002). Osteoid thus possesses stiffness in the same range that we find MSCs take on the shape and expression profiles of an osteogenic lineage (25–40 kPa in Figures 1B and 1C).

Cytoskeletal Markers and Transcription Factors also Indicate Lineage Specification

Immunostaining of cytoskeletal markers and transcription factors across the range of matrix stiffnesses (Figure 3A) proves consistent with the lineage profiling of Figure 1. On the softest, neurogenic matrices, a majority of cells express β3 tubulin, which, along with P-NFH and NFH, is visible in long, branched extensions but is poorly expressed, if at all, in cells on stiffer gels (Figure 2C). On moderately stiff, myogenic matrices, MSCs upregulate the transcription factor MyoD1, localizing it to the nucleus (large arrow; Figure 3A). Compared with C2C12 myoblasts, transcript levels (Figure 3B; Table S3) as well as fluorescence intensity analyses (Figure 3C) indicate about 50% relative expression levels after 1 week on the myogenic matrix; MSCs on softer and stiffer matrices do not express significant MyoD1 or other muscle markers (e.g., titin, pax-3,7, and myogenin). On the stiffest, osteogenic matrices, MSCs upregulate the transcription factor CBFα1 (Figure 3A; open arrow), which is a crucial early marker of osteogenesis (Gilbert et al., 2002). Compared with hFOB osteoblasts, transcript levels (Figure 3B; Table S3) as well as fluorescence intensity analyses (Figure 3C) again indicate about 50% relative expression levels after 1 week on the osteogenic matrix; MSCs on softer matrices do not express significant CBFα1 or other osteoblast markers (e.g., collagen-1s and BMPs).

Elasticity-directed marker protein expression on the various substrates is summarized in Figure 3C. A single,

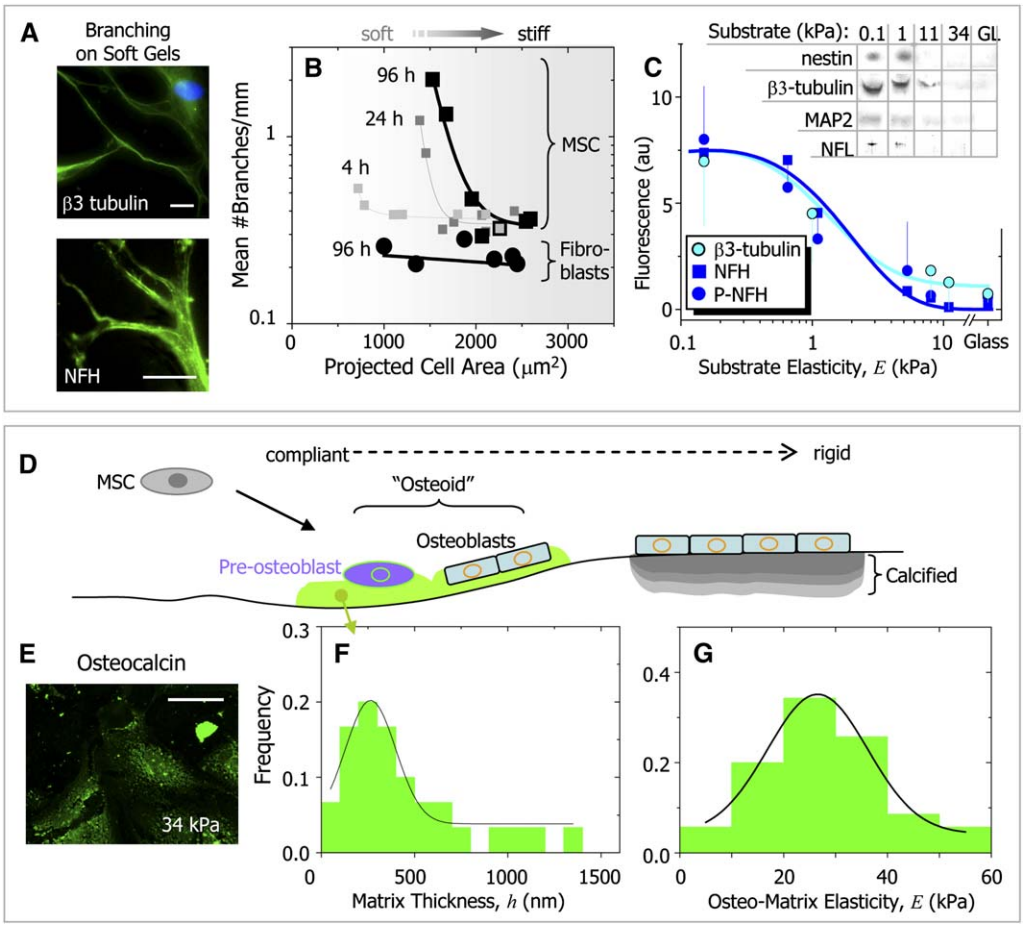

Figure 2. Neurogenic Branching and Osteogenic Microenvironments

(A) Immunofluorescence images of β3 tubulin and NFH in branched extensions of MSCs on soft matrices ($E \sim 1$ kPa). Scale bars are 5 μm.

(B) MSCs and fibroblasts on a range of elastic matrices show an increase in projected area with matrix stiffness, but only MSCs on the softest gels (with smallest areas) show an increasing number of branches per extension length with time.

(C) β3 tubulin, NFH, and P-NFH all localize to the branches of MSCs on the softest substrates with $E < 1$ kPa (mean ± SEM). Nestin, β3 tubulin, MAP2, and NFL Western blotting (inset) confirms expression only on soft gels.

(D) Schematic of the compliant, collagenous "osteoid" microenvironment (green) that MSCs encounter in initial remodeling of bone matrix (adapted from Raisz, 1999). Committed osteoblasts remodel microenvironments by secreting matrix proteins that are slowly calcified.

(E) hFOB osteoblasts secrete osteocalcin after being plated on glass. By day 7, the matrix is thick (F) and compliant with $E_{osteo} \sim 25$–40 kPa (G) based on measurements made by AFM.

nonoverlapping optimum in matrix stiffness after 1 week is seen for the specification of each of the three lineages. The intensity scale is normalized to the primary cells C2C12 and hFOB, which also show optimal matrix elasticities for expression (MyoD and CBFα1, respectively) and further exhibit an elevated baseline in expression on suboptimal matrices. In other words, primary cells appear preprogrammed to express an elevated basal level of the characteristic markers regardless of matrix. In contrast, MSCs express no significant levels of the lineage markers, except of course on the optimal matrices. Blebbistatin again blocks expression of all markers on all matrices (Figure 3C; gray curve), consistent with an inhibition of the cell's ability to feel and respond to its matrix.

Induction Media Adds to Inductive Matrix before Lineage Commitment

In culture, differentiation of MSCs is usually induced by addition of specific soluble factors, such as Dexamethasone, which can permeate cell membranes and can, in principle, directly activate lineage programs. The myoblast induction media used here (MIM, Table S2) is already known to promote myogenesis, with expression of MyoD, Myogenin, and skeletal muscle myosin heavy chain (Gang et al., 2004; Pittenger et al., 1999). Across the various elastic matrices here, MIM induces MSCs to express high basal levels of MyoD that approach the constitutive expression levels of C2C12 myoblasts (Figure 4A). A clear peak for MSC + MIM on the myogenic matrix (8–17 kPa)

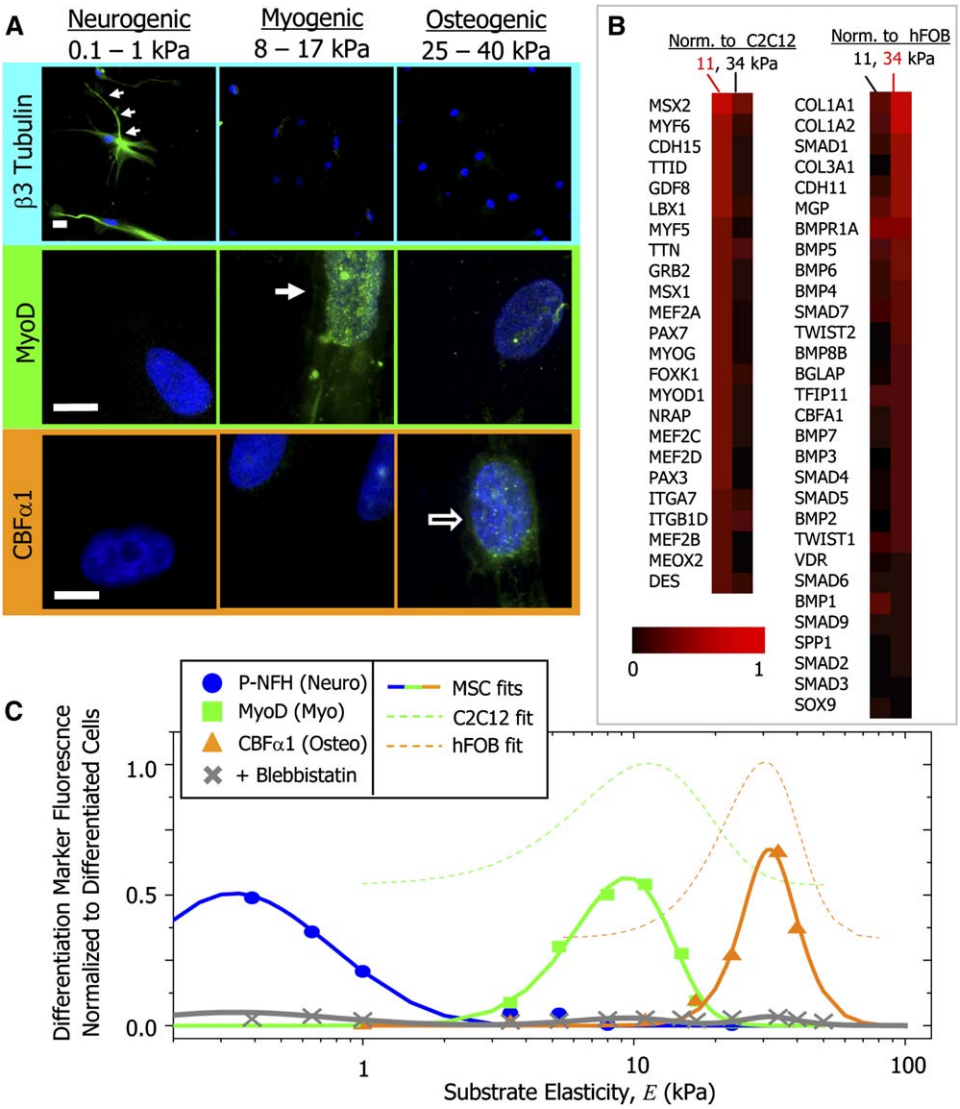

Figure 3. Protein and Transcript Profiles Are Elasticity Dependent under Identical Media Conditions

(A) The neuronal cytoskeletal marker β3 tubulin is expressed in branches (arrows) of initially naive MSCs (>75%) and only on the soft, neurogenic matrices. The muscle transcription factor MyoD1 is upregulated and nuclear localized (arrow) only in MSCs on myogenic matrices. The osteoblast transcription factor CBFα1 (arrow) is likewise expressed only on stiff, osteogenic gels. Scale bar is 5 μm.

(B) Microarray profiles of MSCs cultured on 11 or 34 kPa matrices, with expression normalized first to actin and then to expression of committed C2C12 myoblasts and hFOB osteoblasts.

(C) Fluorescent intensity of differentiation markers versus substrate elasticity reveals maximal lineage specification at the *E* typical of each tissue type. Average intensity is normalized to peak expression of control cells (C2C12 or hFOB), for which only fits to Equation S3 are shown. Blebbistatin blocks all marker expression in MSCs.

is evident and suggests a statistically similar level of lineage commitment for MSCs and C2C12 cells.

Addition of blebbistatin to persistently block NMM II activity (i.e., MIM + blebbistatin) still blocks cell spreading, but MyoD expression is found to be significantly above baseline. However, expression lacks the usual matrix-induced peak expression near E_{muscle} (Figure 4A). Thus, matrix-driven expression changes appear to depend on active NMM II, while induction media stimulates basal-level myogenesis regardless of cell shape or active NMM II. Additionally, when blebbistatin is added to MSCs that are allowed to first spread and become spindle shaped for 24 hr on E_{muscle} gels (see Figure 1B), MSCs maintain their morphology (Figure S2), but the blebbistatin suppresses MyoD expression. Subsequent washout of the drug 72 hr later allows full recovery of MyoD expression. When taken together, (1) lack of MyoD expression by spindle-shaped blebbistatin-treated MSCs, (2) induced

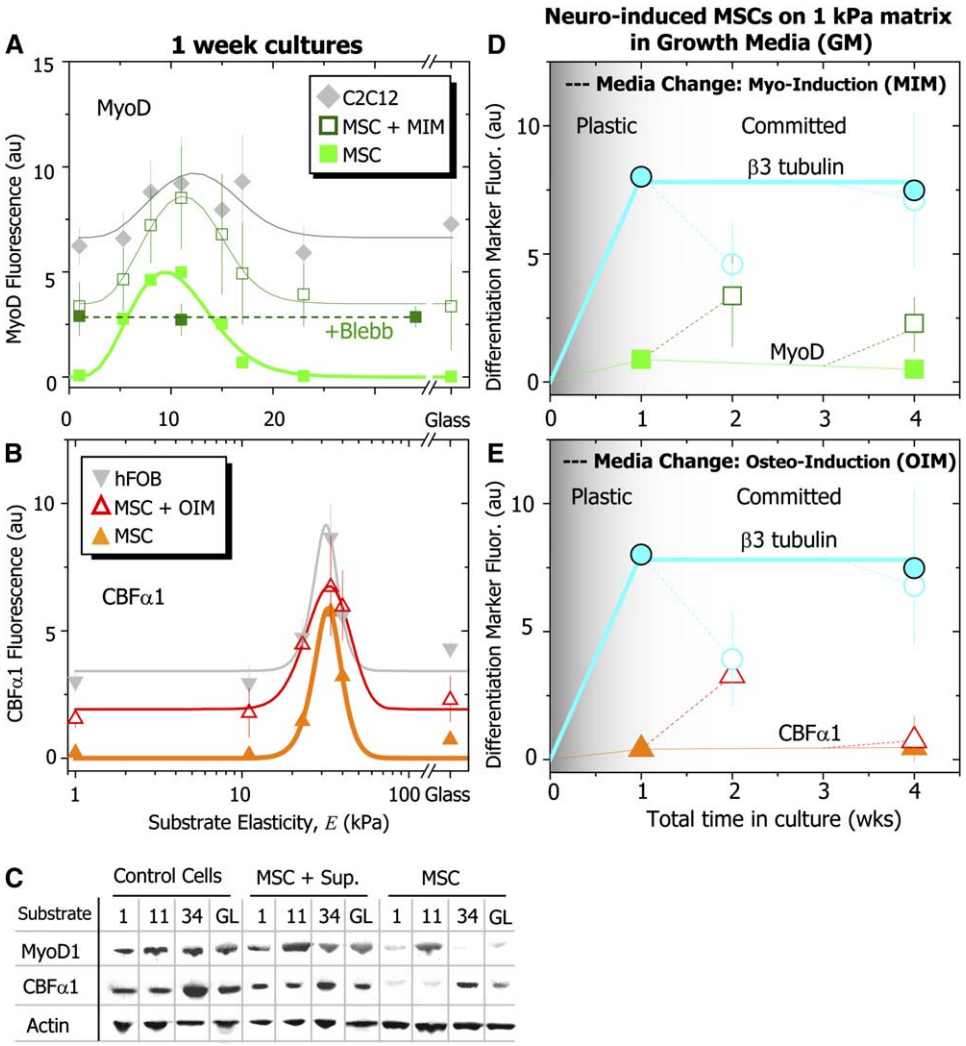

Figure 4. Induction Media and Matrix Reveal Synergy as well as Lineage Plasticity and Eventual Commitment

(A and B) After 1 week in culture in standard MSC growth media, fluorescent intensities of MyoD1 and CBFα1 in MSCs reveal little to no expression except at peaks near E_{muscle} and E_{osteo}, respectively. When myogenic or osteogenic induction media (MIM or OIM) is added, MyoD1 or CBFα1 expression occurs on all substrates, with peak expression at levels near those of control cells, indicating a synergy of matrix and media induction. When cultured in both MIM and blebbistatin (filled symbol and dashed line), MSCs also express a constant level of MyoD. Curve fits throughout use Equation S3.

(C) Western blots confirm lineage specification with matrix or supplemented media alone: when normalized to actin, CBFα1, and MyoD expression reach control levels only when both matrix stiffness and media are conducive for specification.

(D and E) MSCs plated on neurogenic matrices in standard growth media were cultured for 1 or 3 weeks prior to having their media changed to MIM or OIM for an additional week (open data points). After mixed induction for 1 week + 1 week, MSC expression of β3 tubulin is seen to decrease while MyoD1 or CBFα1 expression increases, thus creating *trans*-differentiated cell types when compared to cultures in normal growth media (closed data points). However, after 3 weeks of matrix induction, MSCs become committed and unperturbed by 1 week in *trans*-induction media. Cells remain branched and express the same high levels of β3 tubulin with little to no significant expression of MyoD or CBFα1. Fluorescence intensities (mean ± SEM) were measured for dual-labeled cells.

expression in MIM of unspread cells, and also (3) MIM-induced MyoD expression on "incorrect" matrices (e.g., MSC + MIM on 1 kPa or 34 kPa gels) all imply that active NMM II is indeed important to lineage specification independent of cell shape. It is also clear, however, that on ECM with the "correct" elasticity, active NMM IIs, and soluble induction factors synergistically combine for more complete myogenesis, as calibrated against committed cells (i.e., C2C12).

Similar results as above are found with a standard osteoblast induction media (OIM), which is known to promote cytoskeletal rearrangement and alkaline phosphatase production (Jaiswal et al., 1997; McBeath et al., 2004). Increased basal expression of CBFα1 occurs on all

substrates, and there is still a clear optimum for lineage specification on the stiffest, osteogenic gels (Figure 4B). The quantitative immunofluorescence assessments above are confirmed by Western blots and clearly highlight the precommitted nature of C2C12 and hFOB "control cells" as well as both the constitutive and additive effects of induction media on MSCs (Figure 4C).

The results above indicate that cells grown on a matrix that is, for example, neurogenic due to its softness (1 kPa), can be induced by soluble factors (MIM or OIM) to also express myogenic or osteogenic factors yielding a "mixed MSC phenotype." To assess commitment due to matrix alone, MSCs were preplated in standard growth media for either 1 or 3 weeks on the soft neurogenic gels and then switched to the different induction media. Without the added induction media, cells stably express the neurogenic marker β3 tubulin at a constant level from 1 to 4 weeks (Figures 4B and 4D; closed points). However, when either MIM or OIM is added after 1 week, a further week of culture reduces β3 tubulin levels by about half and increases negligible MyoD levels several-fold (Figures 4B and 4D; open points). These "mixed phenotype" MSCs display multiple lineage signals, albeit at low levels, rather than creating two MSC populations committed to different lineages in the same culture, as cells at this plating concentration are very slow to proliferate, even in growth media (McBeath et al., 2004). In contrast, when MSCs are preincubated for 3 weeks on neurogenic matrices before switching media for a final week, MSCs are less plastic and more firmly committed to their matrix-defined lineage: high levels of β3 tubulin remain statistically the same, and CBFα1 is essentially undetectable. Similar results are also observed for matrix changes where MSCs, replated from stiff to soft matrices, maintain their original specification when given sufficient incubation time (not shown). Slight perturbations under delayed mixed induction might be real (e.g., MyoD upregulation in Figure 4D), since plasticity of "differentiated" cell types has been demonstrated in various systems with (a) chemical agonists that *trans*-differentiate myotubes (Rosania et al., 2000), (b) transfected transcription regulators that *trans*-differentiate fibroblasts to myoblasts (Davis et al., 1987), and (c) classical growth factor pathways that *trans*-differentiate myotubes to osteocytes (Katagiri et al., 1994).

Myosins in MSCs Couple Expression to Matrix Stiffness and Reveal a Key Role for NMM IIs

Forces generated and/or imposed on the cell's actin cytoskeleton have been postulated to influence differentiation (Engler et al., 2004a; Hinz et al., 2001; McBeath et al., 2004), but no past reports have hinted at strong, tissue-directed feedback of microenvironment elasticity on myosin expression or stem cell lineage specification. Cellular tension must be modulated by matrix stiffness, with force transmission occurring via focal adhesions. As described in the introduction and supported by the blebbistatin and ML7 results above, the likely generators of force are the nonmuscle myosin II isoforms. We indeed find that these and a number of myosin transcripts are not only expressed in naive MSC but also upregulated on stiffer gels (11 and 34 kPa) when compared to softer matrices (Figure 5A; left). Western blots and immunofluorescent imaging both confirm array results and show that NMM IIB is up more than 2-fold relative to myosin levels before differentiation (Figures 5B and 5C) on stiff matrices but is downregulated on the softest substrates. It is also found that induction media has comparatively little effect on these stiffness-responsive expression profiles (Figure 5C). The kinetics of NMM IIB imply that it generates higher force than NMM IIA (Rosenfeld et al., 2003) since it spends a greater amount of time strongly attached to actin. We therefore speculate that as matrix stiffness increases, the cell alters its nonmuscle myosin expression in order to generate greater forces on its actin cytoskeleton, which would be necessary to deform a stiffer matrix.

Select myosin genes appear more matrix sensitive than others based on microarray data clustered by RNA variation (Var) (Figure 5A; left). Western blots confirm the variation; NMM IIB expression is more sensitive to matrix elasticity than NMM IIA expression (Figure 5B). The blots also confirm (1) myogenic commitment with requisite upregulation of both MyoD and the intermediate filament protein desmin (Weitzer et al., 1995) and (2) osteogenic commitment with CBFα1. Immunofluorescence images of NMM IIA not only reinforce microarray and blot results but further reveal changes in myosin organization (Figure 5C; inset images). On soft matrices, NMM II staining is diffuse. On moderately stiff matrices, myosin striations emerge that have an appearance previously described as premyofibrillar structures in committed myoblasts (Sanger et al., 2002). Spacing between these nascent striations is the same for MSCs and age-matched C2C12 myocytes (1.0 ± 0.3 μm), and while these striations are lost on the stiffest matrices where stress fibers predominate, NMM II striation appears consistent with nonmuscle myosin organization (Verkhovsky et al., 1995). However, the striation period is clearly smaller than the spacing set by myogenic molecular "rulers" such as titin (TTN in Figure 3B) (Sanger et al., 2002), indicating that MSCs have not assembled mature myofibrils after a week in culture. This is consistent with low levels of skeletal muscle myosin transcript (MHC2A; Figure 5A) and protein (Figure S1B), emphasizing the fact that these sparse cultures of mononucleated MSCs can become committed but remain early myoblasts.

Chronic inhibition of NMM II's ATPase activity with blebbistatin (Limouze et al., 2004; Straight et al., 2003) not only inhibits morphological changes of MSCs on various matrices (Figures 1Bi and 1Bii) but also reduces transcripts levels for NMM IIA (to 50%), IIB (to 8%), and IIC (to 3%) (Figure 5A; right). Importantly, myosins that are not directly affected by blebbistatin treatment changed to a lesser extent from control levels, with one-third of the panel showing no change (MYO5B, MYO1A, MLC3, and MYH3). This highlights the specificity of a key mechanosensing feedback loop between blebbistatin-inhibited activity

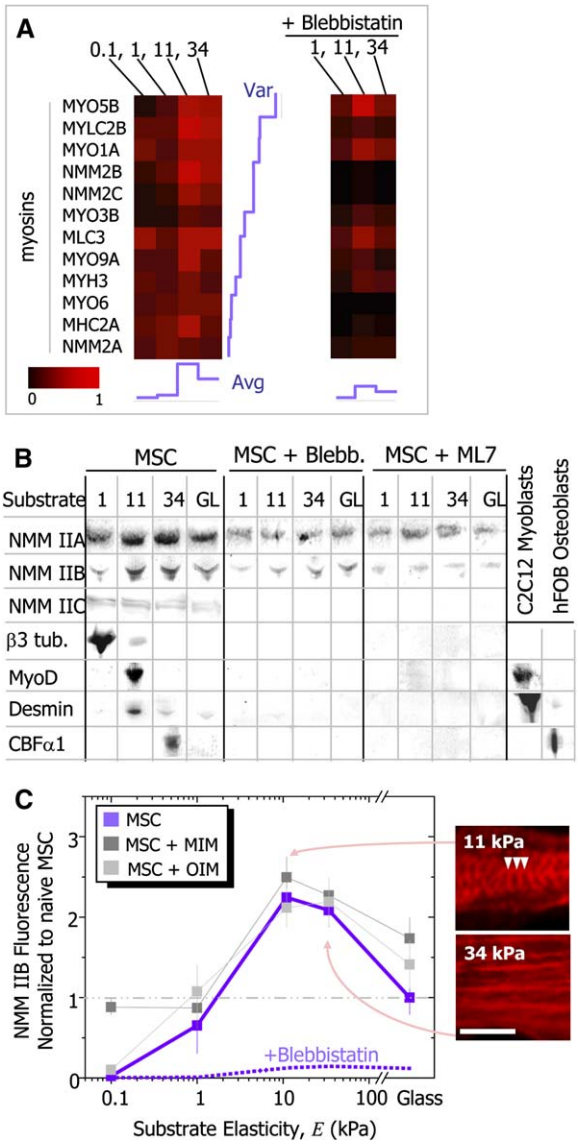

Figure 5. Multiple Myosins Are Expressed by MSCs Dependent on Matrix and Contractility

(A) A range of myosin transcripts show graded sensitivity to stiffness (Var) and an overall average expression (Avg) that is upregulated for MSCs on stiffer matrices. Blebbistatin downregulates many myosin transcripts, especially those for NMM IIB, IIC, and myosin VI, which are directly inhibited.

(B) Immunoblots show large variations with substrate stiffness in NMM IIB, C, and various differentiation markers: neurogenic (β3 tubulin), myogenic (MyoD and Desmin), and osteogenic markers (CBFα1). These also show sensitivity to blebbistatin and ML7.

(C) Immunofluorescence of NMM IIB (mean ± SEM) shows similar stiffness sensitivity and does not change with induction media (i.e. MIM or OIM), but blebbistatin inhibits expression ~10-fold (dashed line) based on Western blots. Inset images of NMM II highlight organization of NMM II with striations (arrowheads) on E_{muscle} matrix (11 kPa) and stress fibers on the stiffer matrix (34 kPa). Scale bar is 5 μm.

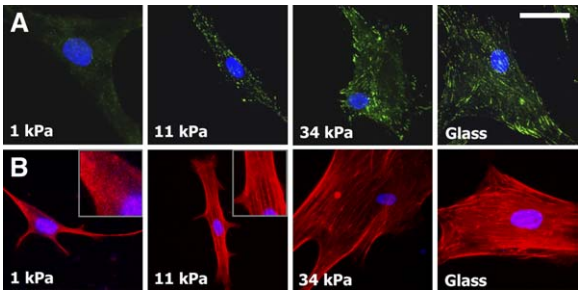

Figure 6. Adhesions Grow and Cytoskeletal Organization Increases with Substrate Stiffness

(A) Paxillin-labeled adhesions grow from undetectable diffuse "contacts" on neurogenic, soft gels (1 kPa) to punctate adhesions on stiffer, myogenic gels (11 kPa). On the stiffest, osteogenic gels (34 kPa), the adhesions are long and thin and slightly more peripheral than they appear on glass.

(B) F-actin organization shows a similar trend, from diffuse on soft gels to progressively organized on stiffer substrates (as stress fibers). Scale bar is 20 μm.

and NMM II expression. Western blots confirm similar isoform sensitivity at the protein level to blebbistatin and also to ML7, an inhibitor that also inhibits the NMM II's through its inhibition of MLCK. NMM IIA expression only slightly downregulates, while NMM IIB expression drops about 10-fold to levels comparable to MSCs on soft gels (Figures 5B and 5C), and NMM IIC is no longer detectable. The downregulation suppresses both striation and stress-fiber formation, consistent with a relaxation effect on blebbistatin-treated cells (Griffin et al., 2004) as well as the crosstalk between nonmuscle myosin II activity and morphogenetic and phenotypic specification. On soft gels, cells generally display less cytoskeletal organization (Engler et al., 2004a; Flanagan et al., 2002), as reinforced with results below. Both blebbistatin and ML7 suppress expression of key lineage markers (Figures 1C and 5B), consistent with NMM II activity, ultimately regulating lineage marker profiles in addition to its own expression.

MSC Focal Adhesions Increase with NMM II-Based Contractility and Both Increase with Matrix Stiffness

Stiff substrates promote focal adhesion growth and elongation, based on paxillin immunofluorescence (Figure 6A). Consistent with this observation, stiff substrates led to increased expression of focal adhesion components (Table S4), including nonmuscle α-actinin, filamin, talin, and focal adhesion kinase (FAK or PTK2). These results with MSCs are fully consistent with the earliest reports of the substrate-stiffness responses of differentiated cells (Pelham and Wang, 1997). We also find that MSCs feel into matrices on the length scales of their adhesions and not much deeper. This is based on the finding that a thin soft gel on glass ($h \sim 0.5$–1 μm) fosters cell spreading similar to that of cells on stiffer gels (Figure S3). Actin assembly follows the trends in adhesion assembly (Figure 6B), which

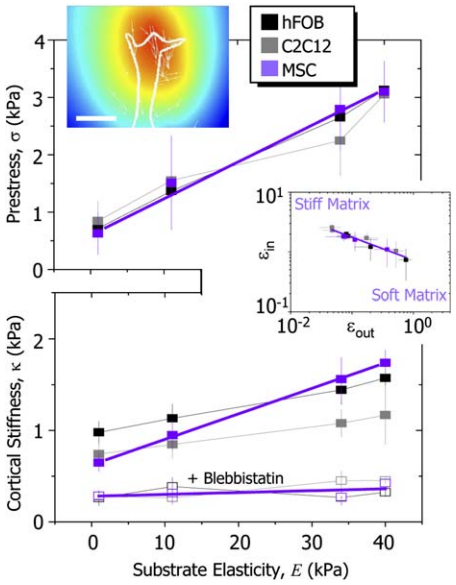

Figure 7. Stiffer Matrices Produce Stiffer and More Tense Cells

Cell prestress, σ, in both MSCs and control cell lines increases linearly with substrate elasticity, E. Inset image shows a myoblast (outlined) displacing beads embedded in the gel (white arrows) that equates to a strain field represented by the color map (red is high strain). Scale bar is 10 μm. Lower plot shows membrane cortical stiffness measured by micropipette aspiration increases with gel stiffness, but blebbistatin treatment softens all cell membranes >3-fold. Middle inset shows mean intracellular strain, ε_{in} ($\sim \sigma / \kappa$), versus the mean extracellular strain, ε_{out} ($\sim \tau / E$), fit to a power law (i.e., $\varepsilon_{in} = B\,\varepsilon_{out}^{b}$) for all cell types. The trend implies larger deformation within the cell on stiff matrices and larger deformation in the matrix on softer matrices. Results shown are Mean ± SEM.

generalizes the matrix-driven assembly of the cytoskeleton to MSCs. NMM II is already known to promote the assembly of focal adhesions (Conti et al., 2004), and so the prominent adhesions on stiffer substrates is consistent with greater activity of NMM II.

Focal adhesions provide MSCs the necessary force transmission pathways to "feel" their microenvironment through actin-myosin contractions. This pulling or contractility by cells can be measured as a mean cellular prestress, σ, that balances the traction stresses, τ, exerted on the gel by the cell (Wang et al., 2002) (Figure 7). Consistent with monotonic increases in focal adhesions versus matrix stiffness, the prestress σ for MSCs, C2C12 myoblasts, and hFOB osteoblasts all show a linear increase versus matrix stiffness (Figure 7; top). Blebbistatin prevents any of the cells from developing either a prestress σ (Griffin et al., 2004) or—as measured by a single-cell micropipette aspiration method (Figure S4)—a significant cell cortex stiffness κ on any matrix (Figure 7; bottom, open points). The simplistic measures here of cell mechanics demonstrate that stiffer matrices produce stiffer and increasingly tensed cells.

DISCUSSION

Lineage specification of naive stem cells induced by soluble stimuli has been well described (Gang et al., 2004; Jaiswal et al., 1997; McBeath et al., 2004; Pittenger et al., 1999), but the results here report a strong and previously undocumented influence of microenvironment stiffness on stem cell specification. Naive stem cells express no baseline levels of lineage-specific markers, in contrast to committed cells (myoblasts and osteoblasts in Figures 3B, 3C, 4A, and 4B), so that—against this low baseline—MSCs are seen to respond dramatically in both morphology and lineage to the matrix presented. The responses here do not include remodeling the microenvironment; for example, collagen-I production is very low in MSCs on soft matrices <11 kPa (see downregulated matrix transcripts; Figure 1C), whereas on 34 kPa matrices, MSCs appear somewhat more secretory (e.g., BMP1-5 and COL3A1), consistent with the secreting hFOB osteoblasts (Figure 2E) (Kong et al., 2005). This passive, initial response of MSCs to the microenvironment would be expected from a multipotent stem cell awaiting instruction.

MSC plasticity is evident in the initial responsiveness to conflicting signals from soft matrix and media (Figures 4D and 4E), consistent with passive responsiveness to inputs. The slow time course of true lineage commitment here contrasts with the rapid and controversial morphological changes with DMSO (Dinsmore et al., 1996; Woodbury et al., 2002). Here, MSCs spread with time, and branching increases on soft matrices (Figure 2B), indicating an active process. In contrast, fibroblasts (Figure 2B), myoblasts (Engler et al., 2004a), and osteoblasts (not shown) do not appear branched on soft substrates. The committed differentiation of the latter cell types (epigenetic) to specified lineages precludes, for example, the reprogramming of myosin levels with changes of matrix (Table S4). In comparison, MSCs prove far more responsive, and while evidence for roles of nonmuscle myosins in MSCs feeling the matrix is suggestive, more work on mechanism is clearly needed.

Possible Implications for Stem Cell Therapies

Regenerative applications of stem cells are being investigated for a number of tissues, including clinical trials for postmyocardial infarction patients (Lee et al., 2004). Efficacy appears uncertain or mixed (Murry et al., 2004), and recent findings have raised the possibility that the injured microenvironment loses compliance with fibrotic scarring, producing a noninducing environment (Berry et al., 2006) that, as we show here, stem cells cannot sufficiently remodel. The results here suggest the need for optimizing matrix elasticity to foster regeneration, which seems applicable to a number of regenerative applications of stem cells such as cardiomyoplasty, muscular dystrophy, and neuroplasty. Any starting point for such approaches must include characterization of the mechanosensitivity of the stem cell of interest to matrix elasticity.

The results of this study also suggest that "precommitting" stem cells to a specific lineage via appropriate in vitro matrix conditions might partially overcome an inappropriate in vivo microenvironment.

EXPERIMENTAL PROCEDURES

Cell Culture

Human Mesenchymal Stem Cells (MSCs; Osiris Therapeutics; Baltimore, MD), human osteoblasts (hFOBs, ATCC), primary human skin fibroblasts (1F7) (Engler et al., 2004a), and murine myoblasts (C2C12s, ATCC) were cultured in normal growth media listed in Table S2. To chemically induce differentiation, cells were placed in the appropriate induction media also listed. All cells were used at low passage numbers, were subconfluently cultured, and were plated at $\sim 10^3$ cells/cm^3 for experiments. Cells were cultured for 7 days or cultured and replated for a specified time unless otherwise noted. All chemicals were purchased from Sigma (St. Louis, MO) unless otherwise noted. To inhibit proliferation, cells were exposed to mitomycin C (10 μg/ml) for 2 hr and washed three times with media prior to plating. Blebbistatin (50 μM, EMD Biosciences), a nonmuscle myosin II inhibitor, was applied with every media change and was stable in culture media for up to 48 hr, as determined by thin-layer chromatography. Y27632 (10 μM, EMD Biosciences), a ROCK inhibitor, and ML7 (10 μM; EMD Biosciences), a myosin light chain kinase inhibitor, were also added to inhibit specification.

Substrate Preparation

Cells were plated on variably compliant polyacrylamide gels, according to a previously established protocol by Pelham and Wang (Pelham and Wang, 1997), creating gels that were ~70–100 μm thick as measured by microscopy. To produce thin gels, a protocol from Engler and coworkers was used (Engler et al., 2004b). Type 1 collagen was used at 0.25–1 μg/cm^2 (BD Biosciences), as quantified using fluorescent collagen for calibration (per Engler et al., 2004a).

AFM for Matrix Elasticity and Cell Mechanics Methods

Substrate elasticity was characterized per Engler et al. (2004b). For matrix secreted by hFOB osteoblasts, cells were plated for 7 days on glass substrates to allow matrix deposition. Samples were placed on an Asylum 1-D atomic force microscopy (AFM) (Asylum Research; Santa Barbara, CA) and indented by a pyramid-tipped probe (Veeco; Santa Barbara, CA) with a constant, k_{sp} ~60 pN/nm. Force-indentation profiles were obtained immediately adjacent to a cell, and each indentation profile was fit up to the point at which probe indentation into the secreted matrix stopped with a Hertz cone model (Rotsch et al., 1999). Details of the cell mechanics measurements can be found in the Supplemental Data.

Lineage Specification Assays

Morphological Changes and Immunofluorescence

Changes in cell shape (<4 days), especially the development of branches (Flanagan et al., 2002) or spindle-like morphologies (Engler et al., 2004a), were quantified either by the number of membrane branches per mm of cell or by a "spindle factor," the major/minor cell axis, respectively. Cells also were stained with lineage-specific antibodies: myogenesis with Myogenesis Differentiation Protein 1 (MyoD1; Chemicon) and desmin (Sigma); osteogenesis with Core Binding Factor α1 (CBFA1; Alpha Diagnostic International) and osteocalcin (EMD Biosciences); and neurogenesis with phosphorylated and dephosphorylated Neurofilament Heavy chain (NFH; Sternberger Monoclonal), Neurofilament Light chain (NFL; Sigma), nestin (BD Pharmagen), Microtubule Associated Protein 2 (MAP2; Chemicon), and β3 tubulin (Sigma) along with paxillin (Chemicon), skeletal muscle myosin heavy chain (Zymed), nonmuscle myosin IIA and IIB (Sigma), IIC (courtesy of R. Adelstein, NIH), and rhodamine-labeled phalloidin. Cells were fixed, blocked, permeabilized, and labeled with Hoechst 33342, primary and secondary antibodies, or 60 μg/ml TRITC-phalloidin.

Cell morphology and fluorescently labeled cells were examined on a TE300 inverted epifluorescent Nikon or Olympus (TIRF) microscope, imaged on a Cascade CCD camera (Photometrics), and quantified with Scion Image. Intensity analysis was displayed as the fold-change of the whole cell average above background fluorescence and staining with secondary antibodies only. For Figure 3C only, however, intensities were then normalized by the maximal expression of the positive control cell. For Figure 5C only, intensities were then normalized by the expression of initially isolated MSCs to show a change from the initial myosin level.

Western Blotting

Cells were plated on gels on 45 × 50 sq. mm coverslips to obtain enough cells for Western blotting. Cells were permeablized (1:1 of 10% SDS, 25 mM NaCl, 10 nM pepstatin, and 10 nM leupeptin in distilled water and loading buffer), boiled for 10 min, and placed in reducing PAGE (Invitrogen). Proteins were transferred onto nitrocellulose, blocked, and labeled via HRP-conjugated antibodies (Biorad). All Westerns were run in duplicate, along with an additional blot for actin and Coomassie blue staining to ensure constant protein load among samples.

Oligonucleotide Array Assays

Total RNA (3–5 μg) was obtained from MSCs cultured on gel substrates of varying stiffness, as well as C2C12 myoblasts and hFOB osteoblasts, using an ethanol-spin column extraction. Samples were labeled with an Ampolabeling Linear Polymerase Reaction kit (SuperArray Bioscience) and hybridized to custom oligonucleotide arrays. Chemiluminescent signals were detected on Biomax Film (Kodak). Arrays were first corrected for array background fluorescence and normalized to a control gene, β-actin. Data for genes indicating mesenchymal origin (Table S1) along with genes for contractile, adhesive, and activating proteins (Table S4) were displayed only as this actin-normalized value. Genes for neuro-, myo-, and osteogenesis, however, were further analyzed by either (1) comparing MSCs on gels to initially isolated MSCs (Figure 1C and Table S3; i.e., [MSC on specific gel]/[initially isolated MSC]) or (2) normalizing MSC expression on gels to control cell expression level (Figure 3B and Table S3; i.e., [MSC on specific gel]/[control cell]).

Supplemental Data

Supplemental Data include four figures, four tables, experimental procedures, and references and can be found with this article online at http://www.cell.com/cgi/content/full/126/4/677/DC1/.

ACKNOWLEDGMENTS

We gratefully acknowledge Drs. Jean and Joe Sanger, Dr. Paul Janmey, Dr. Jonathan Raper, Dr. Masaki Noda, Dr. Louis, and Dr. Robert Adelstein for reagents and discussions. Support was provided by grants from NIAMS (H.L.S. and D.D.), NHLBI and NIBIB (D.D.), MDA (H.L.S. and D.D.), NSF (D.D.), NSF-MRSEC, and the Ashton Foundation. (A.E.).

Received: November 1, 2005
Revised: March 7, 2006
Accepted: June 6, 2006
Published: August 24, 2006

REFERENCES

Alenghat, F.J., and Ingber, D.E. (2002). Mechanotransduction: all signals point to cytoskeleton, matrix, and integrins. Sci. STKE *119*, PE6.

Allingham, J.S., Smith, R., and Rayment, I. (2005). The structural basis of blebbistatin inhibition and specificity for myosin II. Nat. Struct. Mol. Biol. *12*, 378–379.

Andrades, J.A., Santamaria, J.A., Nimni, M.E., and Becerra, J. (2001). Selection and amplification of a bone marrow cell population and its induction to the chondro-osteogenic lineage by rhOP-1: an in vitro and in vivo study. Int. J. Dev. Biol. *45*, 689–693.

Beningo, K.A., Dembo, M., Kaverina, I., Small, J.V., and Wang, Y.L. (2001). Nascent focal adhesions are responsible for the generation of strong propulsive forces in migrating fibroblasts. J. Cell Biol. *153*, 881–888.

Berry, M.F., Engler, A.J., Woo, Y.J., Pirolli, T.J., Bish, L.T., Bell, P., Jayasankar, V., Morine, K.J., Gardner, T.J., Discher, D.E., and Sweeney, H.L. (2006). Mesenchymal stem cell injection after myocardial infarction improves myocardial compliance. Am. J. Physiol. Heart Circ. Physiol. *290*, H2196–H2203.

Bershadsky, A.D., Balaban, N.Q., and Geiger, B. (2003). Adhesion-dependent cell mechanosensitivity. Annu. Rev. Cell Dev. Biol. *19*, 677–695.

Conti, M.A., Even-Ram, S., Liu, C., Yamada, K.M., and Adelstein, R.S. (2004). Defects in cell adhesion and the visceral endoderm following ablation of nonmuscle myosin heavy chain II-A in mice. J. Biol. Chem. *279*, 41263–41266.

Cukierman, E., Pankov, R., Stevens, D.R., and Yamada, K.M. (2001). Taking cell-matrix adhesions to the third dimension. Science *294*, 1708–1712.

Davis, R.L., Weintraub, H., and Lassar, A.B. (1987). Expression of a single transfected cDNA converts fibroblasts to myoblasts. Cell *51*, 987–1000.

Deng, J., Petersen, B.E., Steindler, D.A., Jorgensen, M.L., and Laywell, E.D. (2005). Mesenchymal stem cells spontaneously express neural proteins in culture and are neurogenic after transplantation. Stem Cells *24*, 1054–1064.

Dhawan, J., and Helfman, D.M. (2004). Modulation of acto-myosin contractility in skeletal muscle myoblasts uncouples growth arrest from differentiation. J. Cell Sci. *117*, 3735–3748.

Dinsmore, J., Ratliff, J., Deacon, T., Pakzaban, P., Jacoby, D., Galpern, W., and Isacson, O. (1996). Embryonic stem cells differentiated in vitro as a novel source of cells for transplantation. Cell Transplant. *5*, 131–143.

Discher, D.E., Janmey, P.A., and Wang, Y.-L. (2005). Tissue cells feel and respond to the stiffness of their substrate. Science *310*, 1139–1143.

Engler, A.J., Griffin, M.A., Sen, S., Bonnemann, C.G., Sweeney, H.L., and Discher, D.E. (2004a). Myotubes differentiate optimally on substrates with tissue-like stiffness: pathological implications for soft or stiff microenvironments. J. Cell Biol. *166*, 877–887.

Engler, A.J., Richert, L., Wong, J.Y., Picart, C., and Discher, D.E. (2004b). Surface probe measurements of the elasticity of sectioned tissue, thin gels and polyelectrolyte multilayer films: correlations between substrate stiffness and cell adhesion. Surf. Sci. *570*, 142–154.

Ferrari, G., Cusella-De Angelis, G., Coletta, M., Paolucci, E., Stornaiuolo, A., Cossu, G., and Mavilio, F. (1998). Muscle regeneration by bone marrow-derived myogenic progenitors. Science *279*, 1528–1530.

Flanagan, L.A., Ju, Y.E., Marg, B., Osterfield, M., and Janmey, P.A. (2002). Neurite branching on deformable substrates. Neuroreport *13*, 2411–2415.

Gang, E.J., Jeong, J.A., Hong, S.H., Hwang, S.H., Kim, S.W., Yang, I.H., Ahn, C., Han, H., and Kim, H. (2004). Skeletal myogenic differentiation of mesenchymal stem cells isolated from human umbilical cord blood. Stem Cells *22*, 617–624.

Garcia, A.J., and Reyes, C.D. (2005). Bio-adhesive surfaces to promote osteoblast differentiation and bone formation. J. Dent. Res. *84*, 407–413.

Georges, P.C., Miller, W.J., Meaney, D.F., Sawyer, E., and Janmey, P.A. (2006). Matrices with compliance comparable to that of brain tissue select neuronal over glial growth in mixed cortical cultures. Biophys J. *90*, 3012–3018.

Gilbert, L., He, X., Farmer, P., Rubin, J., Drissi, H., van Wijnen, A.J., Lian, J.B., Stein, G.S., and Nanes, M.S. (2002). Expression of the osteoblast differentiation factor RUNX2 (Cbfa1/AML3/Pebp2alpha A) is inhibited by tumor necrosis factor-alpha. J. Biol. Chem. *277*, 2695–2701.

Griffin, M.A., Sen, S., Sweeney, H.L., and Discher, D.E. (2004). Adhesion-contractile balance in myocyte differentiation. J. Cell Sci. *117*, 5855–5863.

Hinz, B., Celetta, G., Tomasek, J.J., Gabbiani, G., and Chaponnier, C. (2001). Alpha-smooth muscle actin expression upregulates fibroblast contractile activity. Mol. Biol. Cell *12*, 2730–2741.

Hofstetter, C.P., Schwarz, E.J., Hess, D., Widenfalk, J., El Manira, A., Prockop, D.J., and Olson, L. (2002). Marrow stromal cells form guiding strands in the injured spinal cord and promote recovery. Proc. Natl. Acad. Sci. USA *99*, 2199–2204.

Holmbeck, K., Bianco, P., Caterina, J., Yamada, S., Kromer, M., Kuznetsov, S.A., Mankani, M., Robey, P.G., Poole, A.R., Pidoux, I., et al. (1999). MT1-MMP-deficient mice develop dwarfism, osteopenia, arthritis, and connective tissue disease due to inadequate collagen turnover. Cell *99*, 81–92.

Jaiswal, N., Haynesworth, S.E., Caplan, A.I., and Bruder, S.P. (1997). Osteogenic differentiation of purified, culture-expanded human mesenchymal stem cells in vitro. J. Cell. Biochem. *64*, 295–312.

Katagiri, T., Yamaguchi, A., Komaki, M., Abe, E., Takahashi, N., Ikeda, T., Rosen, V., Wozney, J.M., Fujisawa-Sehara, A., and Suda, T. (1994). Bone morphogenetic protein-2 converts the differentiation pathway of C2C12 myoblasts into the osteoblast lineage. J. Cell Biol. *127*, 1755–1766.

Katayama, Y., Battista, M., Kao, W.-M., Hidalgo, A., Peired, A.J., Thomas, S.A., and Frenette, P.S. (2006). Signals from the sympathetic nervous system regulate hematopoietic stem cell egress from bone marrow. Cell *124*, 407–421.

Kim, K.Y., Kovacs, M., Kawamoto, S., Sellers, J.R., and Adelstein, R.S. (2005). Disease-associated mutations and alternative splicing alter the enzymatic and motile activity of nonmuscle myosins II-B and II-C. J. Biol. Chem. *280*, 22769–22775.

Kondo, T., Johnson, S.A., Yoder, M.C., Romand, R., and Hashino, E. (2005). Sonic hedgehog and retinoic acid synergistically promote sensory fate specification from bone marrow-derived pluripotent stem cells. Proc. Natl. Acad. Sci. USA *102*, 4789–4794.

Kong, H.J., Polte, T.R., Alsberg, E., and Mooney, D.J. (2005). FRET measurements of cell-traction forces and nano-scale clustering of adhesion ligands varied by substrate stiffness. Proc. Natl. Acad. Sci. USA *102*, 4300–4305.

Lariviere, R.C., and Julien, J.P. (2004). Functions of intermediate filaments in neuronal development and disease. J. Neurobiol. *58*, 131–148.

Lee, M.S., Lill, M., and Makkar, R.R. (2004). Stem cell transplantation in myocardial infarction. Rev. Cardiovasc. Med. *5*, 82–98.

Limouze, J., Straight, A.F., Mitchison, T.J., and Sellers, J.R. (2004). Specificity of Blebbistatin, an inhibitor of myosin II. J. Muscle Res. Cell Motil. *25*, 337–341.

Lo, C.M., Wang, H.B., Dembo, M., and Wang, Y.L. (2000). Cell movement is guided by the rigidity of the substrate. Biophys. J. *79*, 144–152.

Maitra, A., Arking, D.E., Shivapurkar, N., Ikeda, M., Stastny, V., Kassauei, K., Sui, G., Cutler, D.J., Liu, Y., Brimble, S.N., Noaksson, K., Hyllner, J., Schulz, T.C., Zeng, X., Crook, J., Abraham, S., Colman, A., Sartiny, P., Matsui, S., Carpenter, M., Gazdar, A.F., Rao, M., and Chakravarti, A. (2005). Genomic alterations in cultured human embryonic stem cells. Nat Genet. *37*, 1099–1103.

McBeath, R., Pirone, D.M., Nelson, C.M., Bhadriraju, K., and Chen, C.S. (2004). Cell shape, cytoskeletal tension, and RhoA regulate stem cell lineage commitment. Dev. Cell *6*, 483–495.

Morinobu, M., Ishijima, M., Rittling, S.R., Tsuji, K., Yamamoto, H., Nifuji, A., Denhardt, D.T., and Noda, M. (2003). Osteopontin expression in osteoblasts and osteocytes during bone formation under mechanical stress in the calvarial suture in vivo. J. Bone Miner. Res. *18*, 1706–1715.

Murry, C.E., Soonpaa, M.H., Reinecke, H., Nakajima, H., Nakajima, H.O., Rubart, M., Pasumarthi, K.B.S., Ismail Virag, J., Bartelmez, S.H., Poppa, V., et al. (2004). Haematopoietic stem cells do not transdifferentiate into cardiac myocytes in myocardial infarcts. Nature *428*, 664–668.

Nakagawa, S., Pawelek, P., and Grinnell, F. (1989). Extracellular matrix organization modulates fibroblast growth and growth factor responsiveness. Exp. Cell Res. *182*, 572–582.

Neuhuber, B., Gallo, G., Howard, L., Kostura, L., Mackay, A., and Fischer, I. (2004). Reevaluation of in vitro differentiation protocols for bone marrow stromal cells: disruption of actin cytoskeleton induces rapid morphological changes and mimics neuronal phenotype. J. Neurosci. Res. *77*, 192–204.

Pelham, R.J., and Wang, Y.-L. (1997). Cell locomotion and focal adhesions are regulated by substrate flexibility. Proc. Natl. Acad. Sci. USA *94*, 13661–13665.

Pittenger, M.F., Mackay, A.M., Beck, S.C., Jaiswal, R.K., Douglas, R., Mosca, J.D., Moorman, M.A., Simonetti, D.W., Craig, S., and Marshak, D.R. (1999). Multilineage potential of adult human mesenchymal stem cells. Science *284*, 143–147.

Raisz, L.G. (1999). Physiology and pathophysiology of bone remodeling. Clin. Chem. *45*, 1353–1358.

Rattner, A., Sabido, O., Le, J., Vico, L., Massoubre, C., Frey, J., and Chamson, A. (2000). Mineralization and alkaline phosphatase activity in collagen lattices populated by human osteoblasts. Calcif. Tissue Int. *66*, 35–42.

Roeder, B.A., Kokini, K., Sturgis, J.E., Robinson, J.P., and Voytik-Harbin, S.L. (2002). Tensile mechanical properties of three-dimensional type I collagen extracellular matrices with varied microstructure. J. Biomech. Eng. *124*, 214–222.

Rosania, G.R., Chang, Y.T., Perez, O., Sutherlin, D., Dong, H., Lockhart, D.J., and Schultz, P.G. (2000). Myoseverin, a microtubule-binding molecule with novel cellular effects. Nat. Biotechnol. *18*, 304–308.

Rosenfeld, S.S., Xing, J., Chen, L.Q., and Sweeney, H.L. (2003). Myosin IIb is unconventionally conventional. J. Biol. Chem. *278*, 27449–27455.

Rotsch, C., Jacobson, K., and Radmacher, M. (1999). Dimensional and mechanical dynamics of active and stable edges in motile fibroblasts investigated by using atomic force microscopy. Proc. Natl. Acad. Sci. USA *96*, 921–926.

Rutishauser, U. (1984). Developmental biology of a neural cell adhesion molecule. Nature *310*, 549–554.

Sanger, J., Chowrashi, P., Shaner, N., Spalthoff, S., Wang, J., Freeman, N., and Sanger, J. (2002). Myofibrillogenesis in skeletal muscle cells. Clin. Orthop. Relat. Res. *403S*, S153–S162.

Straight, A.F., Cheung, A., Limouze, J., Chen, I., Westwood, N.J., Sellers, J.R., and Mitchison, T.J. (2003). Dissecting temporal and spatial control of cytokinesis with a myosin II Inhibitor. Science *299*, 1743–1747.

Tamada, M., Sheetz, M.P., and Sawada, Y. (2004). Activation of a signaling cascade by cytoskeleton stretch. Dev. Cell *7*, 709–718.

Tomasek, J.J., Gabbiani, G., Hinz, B., Chaponnier, C., and Brown, R.A. (2002). Myofibroblasts and mechano-regulation of connective tissue remodelling. Nat. Rev. Mol. Cell Biol. *3*, 349–363.

Verkhovsky, A.B., Svitkina, T.M., and Borisy, G.G. (1995). Myosin II filament assemblies in the active lamella of fibroblasts: their morphogenesis and role in the formation of actin filament bundles. J. Cell Biol. *131*, 989–1002.

Wang, N., Tolic-Norrelykke, I.M., Chen, J., Mijailovich, S.M., Butler, J.P., Fredberg, J.J., and Stamenovic, D. (2002). Cell prestress. I. Stiffness and prestress are closely associated in adherent contractile cells. Am. J. Physiol. Cell Physiol. *282*, C606–C616.

Weitzer, G., Milner, D.J., Kim, J.U., Bradley, A., and Capetanaki, Y. (1995). Cytoskeletal control of myogenesis: a desmin null mutation blocks the myogenic pathway during embryonic stem cell differentiation. Dev. Biol. *172*, 422–439.

Wislet-Gendebien, S., Wautier, F., Leprince, P., and Rogister, B. (2005). Astrocytic and neuronal fate of mesenchymal stem cells expressing nestin. Brain Res. Bull. *68*, 95–102.

Woodbury, D., Reynolds, K., and Black, I.B. (2002). Adult bone marrow stromal stem cells express germline, ectodermal, endodermal, and mesodermal genes prior to neurogenesis. J. Neurosci. Res. *69*, 908–917.

Wozniak, M.A., Desai, R., Solski, P.A., Der, C.J., and Keely, P.J. (2003). ROCK-generated contractility regulates breast epithelial cell differentiation in response to the physical properties of a three-dimensional collagen matrix. J. Cell Biol. *163*, 583–595.

nature materials

ARTICLES

PUBLISHED ONLINE: 10 AUGUST 2014 | DOI: 10.1038/NMAT4051

Interplay of matrix stiffness and protein tethering in stem cell differentiation

Jessica H. Wen[1†], Ludovic G. Vincent[1†], Alexander Fuhrmann[1], Yu Suk Choi[1‡], Kolin C. Hribar[2], Hermes Taylor-Weiner[1], Shaochen Chen[2] and Adam J. Engler[1,3*]

Stem cells regulate their fate by binding to, and contracting against, the extracellular matrix. Recently, it has been proposed that in addition to matrix stiffness and ligand type, the degree of coupling of fibrous protein to the surface of the underlying substrate, that is, tethering and matrix porosity, also regulates stem cell differentiation. By modulating substrate porosity without altering stiffness in polyacrylamide gels, we show that varying substrate porosity did not significantly change protein tethering, substrate deformations, or the osteogenic and adipogenic differentiation of human adipose-derived stromal cells and marrow-derived mesenchymal stromal cells. Varying protein–substrate linker density up to 50-fold changed tethering, but did not affect osteogenesis, adipogenesis, surface–protein unfolding or underlying substrate deformations. Differentiation was also unaffected by the absence of protein tethering. Our findings imply that the stiffness of planar matrices regulates stem cell differentiation independently of protein tethering and porosity.

The stiffness of the extracellular matrix (ECM) has been shown to regulate both short- and longer-term cell functions such as cell spreading[1] and stem- and progenitor- cell phenotype changes on planar substrates[2–7]. For example, many types of adult stromal cell grown on substrates of stiffness similar to that of the osteoid or muscle express lineage markers of terminally differentiated cells found in those tissues[3,4,6]. Common myosin-based contractile mechanisms are needed for matrix-induced differentiation in two dimensions[3,8–10]. However, in three dimensions, a labile[11] or degradable matrix[12], which permits cells to first spread and then adhere to the ECM, is required. Similarly, force-mediated protein unfolding in the ECM *in vivo* regulates cell responses as a function of stiffness[13,14]. Whereas creating three-dimensional matrices has become a widespread approach towards understanding how the matrix affects cell fate, the regulatory role of substrate-anchored fibrous- protein deformations on stem cell fate in two dimensions is still unclear.

Recent literature suggests that the mechanical resistance provided by the ECM, which opposes myosin-based contractility that results in cell signalling and differentiation, could, for planar cultures, arise from protein tethers rather than substrate stiffness[15]. As most synthetic planar matrices are not normally cell- adhesive, an adhesive layer of matrix protein is attached to the hydrogel surface and covalently 'tethered' to the substrate surface at distinct anchoring points. Thus, changing protein–substrate linker density or substrate porosity can vary the length of the fibre segment between two adjacent anchoring points. When a load is applied perpendicularly to the fibre segment, its deflection is directly related to the load applied, fibre stiffness, and the cube of the length of the fibre segment[15,16]. If enough resistance were present in these tethers, stem cells could differentiate independently of substrate stiffness. However, it is unclear what the length of these tethers is and how it compares to substrate deformations[17], which have been implicated in mechanotransduction and hence stem cell differentiation[18]. Thus, it is critical to decouple protein tethering and substrate stiffness to determine whether and how these factors collectively regulate stem cell differentiation.

Tuning hydrogel porosity independently of stiffness

Tuning the ratio of acrylamide monomer and bis-acrylamide crosslinker can change the porosity of the polyacrylamide (PA) hydrogel, that is, the distance between tethering points, while maintaining constant stiffness. To accomplish this, three separate acrylamide/bis-acrylamide formulations were polymerized to yield hydrogels of ~4, ~13 and ~30 kPa (Fig. 1a), which correspond to the stiffness of adipose tissue, muscle and osteoid[2,3,6,19–21], respectively. Differences in volume and mass swelling ratios between each of the hydrogels with similar stiffness suggest significant differences in porosity among each substrate subgroup (Supplementary Fig. 1a,b). The radius of gyration of extended DNA may be used to estimate the effective maximum pore size of the hydrogel[22]. DNA size standards were exposed to an electrophoretic gradient in swollen and unconfined 4 and 30 kPa PA hydrogels to further quantify hydrated pore size. For 30 kPa hydrogels, a 45 nm DNA fragment failed to migrate through the 8/0.55 formulation, indicating that the maximum pore size of this formulation is between 23 and 45 nm. Larger DNA fragments migrated through the 10/0.3 and 20/0.15 gel formulations, indicating that the approximate pore sizes are between 88 and 166 nm for both formulations; differences in DNA mobility suggest that the two gels have pore sizes that differ within this range. Similarly, differences in DNA mobility suggest that the three 4 kPa formulations yield hydrogels with different pore sizes (Supplementary Fig. 1c). Scanning electron microscopy (SEM) of dried PA hydrogels showed increasing pore sizes with increasing acrylamide and decreasing bis-acrylamide concentrations for the 4, 13 and 30 kPa hydrogel formulations (Fig. 1b); these data are consistent with pore size trends in hydrated measurements and together demonstrate that

[1]Department of Bioengineering, University of California, San Diego, La Jolla, California 92093, USA, [2]Department of Nanoengineering, University of California, San Diego, La Jolla, California 92093, USA, [3]Sanford Consortium for Regenerative Medicine, La Jolla, California 92037, USA. †These authors contributed equally to this work. ‡Present address: Kolling Institute of Medical Research, Royal North Shore Hospital, The University of Sydney, Sydney, New South Wales 2065, Australia. *e-mail: aengler@ucsd.edu

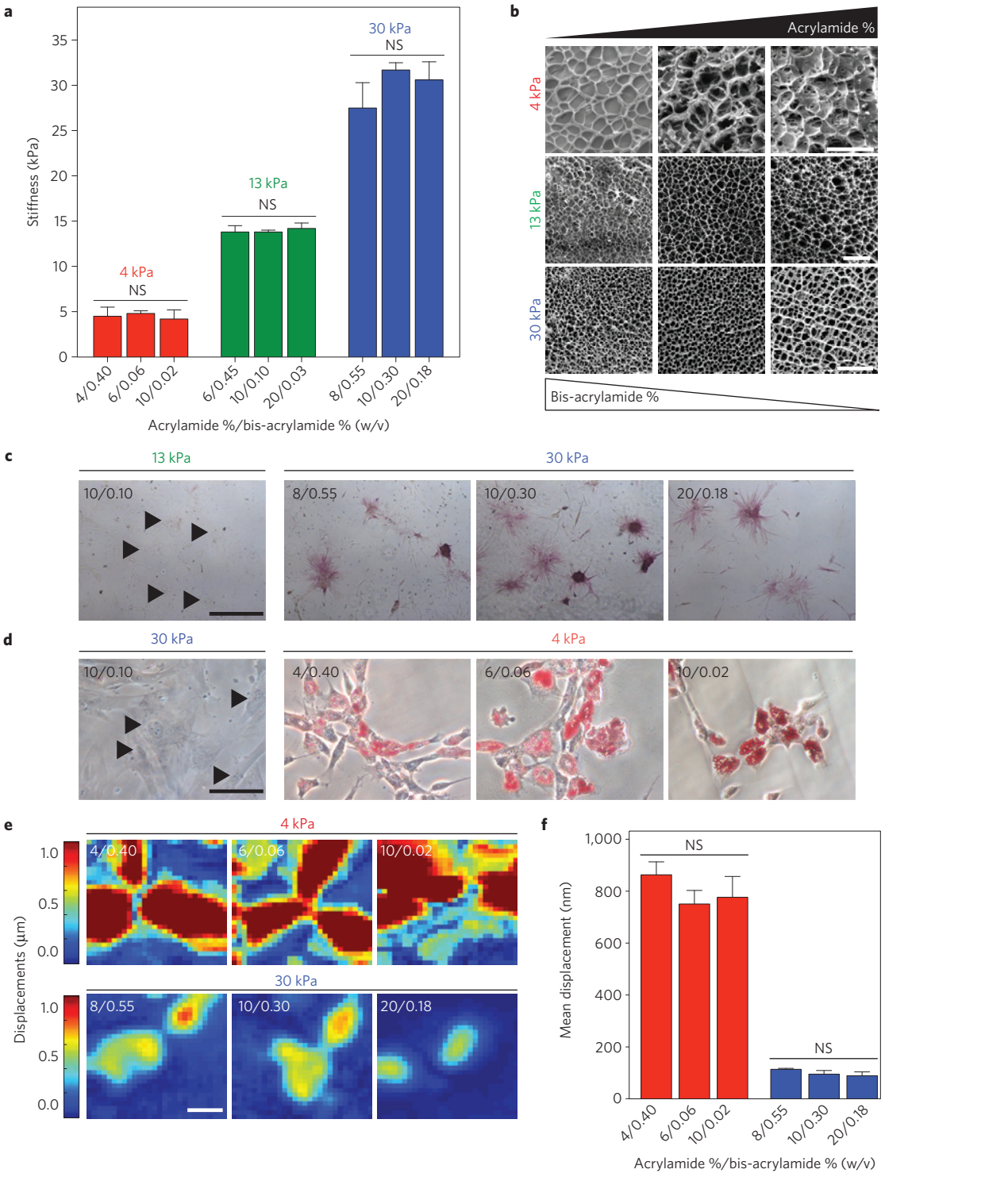

Figure 1 | Influence of substrate porosity on ASC differentiation. a, Elastic modulus measured by AFM ($n=3$) for the indicated acrylamide/bis-acrylamide ratios (mean ± s.d.). **b**, SEM images of PA hydrogels made with varying monomer-to-crosslinker ratios as indicated. Scale bars, 50 μm (top and bottom), 10 μm (middle). **c**, ALP staining of ASCs on 13 and 30 kPa hydrogels of the indicated compositions after 14 days of culture in normal media. Arrowheads indicate stained but yet negative cells. Scale bar, 500 μm. **d**, ORO staining of ASCs on 4 kPa and 30 kPa hydrogels of the indicated compositions after 7 days of culture in adipogenic induction media. Arrowheads indicate stained but yet negative cells. Scale bar, 100 μm. **e**, Displacement maps of embedded fluorescent particles resulting from ASC traction forces on 4 kPa and 30 kPa hydrogels of the indicated compositions. Scale bar, 50 μm. **f**, Quantification of mean displacement was plotted for hydrogels of the indicated composition and stiffness range ($n>20$; mean ± s.e.m.; NS, not significant).

increasing the concentration of the bis-acrylamide crosslinker decreases the relative pore size without substantially changing the modulus of the hydrogel. However, it is important to note here that pore sizes derived from SEM images of freeze-dried hydrogels are probably not representative of actual substrate pore sizes in a hydrated state. Cells interact with hydrated substrates *in vitro*, and thus SEM images are provided only for relative comparison of pore sizes for the hydrogel formulations reported.

Differentiation does not depend on porosity

Human adipose stromal cells (ASCs) were plated onto 13 and 30 kPa PA hydrogels from the formulations indicated in Fig. 1c. After 14 days of culture in normal growth media, osteogenic differentiation (as indicated by positive alkaline phosphatase (ALP) staining in subconfluent cells) occurred regardless of hydrogel formulation and was directly dependent on substrate stiffness, as 13 kPa substrates were negative for ALP (Fig. 1c). Further confirmation of this is demonstrated by positive and nuclear localized RUNX2 immunofluorescence staining after 7 days in culture on all 30 kPa hydrogels (Supplementary Fig. 2a). The expression levels of the early osteogenic markers ALP and RUNX2 suggest that changes in porosity independently of stiffness have no noticeable effects on differentiation for the range of hydrogel formulations tested. However, allowing cells to reach confluence in normal media on any hydrogel formulation was sufficient to override substrate- stiffness-mediated differentiation and induce osteogenesis as previously observed[15], most likely owing to other factors including cell–cell signalling and secreted paracrine factors (Supplementary Fig. 3). To avoid complications arising from confluent monolayers and to focus only on cell–ECM signalling, osteogenic- differentiation studies were conducted at low cell densities. Mesenchymal stromal cells (MSCs), another commonly used cell type in differentiation experiments, also stained positive for ALP after 14 days in culture on the three 30 kPa hydrogel formulations (Supplementary Fig. 3b), implying that substrate porosity has little effect on multiple stem cell types. In addition, after 14 days in culture in adipogenic induction media, adipogenic differentiation, as assessed by oil red O (ORO) presence, was found in over 40% of ASCs on all 4 kPa substrates regardless of hydrogel formulation and was directly dependent on substrate stiffness, as 30 kPa substrates were negative for ORO (Fig. 1d and Supplementary Fig. 2c).

As cell–ECM signalling depends on contractility, and differences in contractility have been shown to regulate differentiation[3,8–10], displacement maps of embedded fluorescent particles resulting from ASC traction forces on all 4 and 30 kPa hydrogel formulations were computed (Fig. 1e and Supplementary Fig. 4) using traction force microscopy[23] (TFM). Mean displacements were similar between all formulations of 4 and 30 kPa hydrogels, but different between hydrogels of different stiffness (Fig. 1f). These data indicate that over the range of formulations tested, hydrogel deformations due to cell contractions are similar regardless of porosity but are dependent on stiffness (Fig. 1e,f). Taken together, these data show that varying porosity alone does not seem to be sufficient to alter the fate of two different adult stem cell sources.

Modulating protein tethering by changing linker density

Culturing cells on synthetic hydrogels requires the covalent coupling of a cell-adhesive matrix protein, such as collagen type I, to the hydrogel surface using a protein–substrate linker, such as sulpho-SANPAH (ref. 1). Changing the concentration of this linker has been proposed to modulate protein tethering[15]. To modulate the tethering of fibrous collagen to PA hydrogels, we tuned the surface density of anchoring points by varying the concentration of sulpho-SANPAH, thus varying the average distance between adjacent anchoring points. To assess possible differences in the physical structure or total amount of bound protein, immunofluorescence staining of collagen covalently coupled to PA substrates activated with varying concentrations of sulpho-SANPAH was performed. Images revealed noticeable surface heterogeneity, making quantification of absolute protein amount difficult (Supplementary Fig. 5a); this was further illustrated by collagen pixel intensity histograms for 13 and 30 kPa hydrogels over a range of sulpho-SANPAH concentrations (Supplementary Fig. 5b). Fluorescent detection was unable to quantify surface-bound protein as previously suggested[15]. To directly quantify collagen tethering, we obtained individual force spectrograms (Supplementary Fig. 6a) from microindentations of collagen-coated PA hydrogels. Substrates activated with a range of sulpho-SANPAH concentrations were indented using a probe functionalized with an anti-collagen type I antibody (Fig. 2a). As the tip retracts from the surface, the collagen unfolds and/or stretches until the antibody–protein bonds rupture (Supplementary Fig. 6a). Force spectrograms were analysed to locate rupture events and to determine the force at rupture, that is, the force required to break a protein–antibody bond, and the rupture length that is, the deflection of the collagen fibre segment at rupture. Larger rupture forces and a greater number of rupture events were detected in the presence of collagen I (Fig. 2b, left and Supplementary Fig. 6b) and indicate that the antibody was specifically binding and loading collagen. Decreasing rupture length with increasing sulpho-SANPAH concentration (Fig. 2b, right) confirmed that the number of protein anchoring points scaled with sulpho-SANPAH concentration without substantial changes in rupture force (Fig. 2b). This trend held for all 30 kPa formulations tested despite significant changes in the number of available protein anchoring sites, which is proportional to acrylamide concentration. We observed differences in rupture length between sulpho-SANPAH concentrations across hydrogel formulations (Fig. 2c, grey versus white bars), indicating that anchoring sites must not be saturated. Furthermore, for a given sulpho-SANPAH concentration, although small differences in average rupture length were detected between the three 30 kPa hydrogel formulations, that is, <40 nm, these differences were smaller than the changes in pore size, which were up to 120 nm (Supplementary Fig. 1c). Thus, differences in rupture lengths between the hydrogel formulations are not likely to be due to porosity changes.

Differentiation does not depend on tethering

To investigate whether or not tethering impacts stem cell fate, subconfluent ASCs and MSCs were cultured in normal growth medium on 30 kPa hydrogels over a range of sulpho-SANPAH concentrations and assessed for osteogenic differentiation. Positive ALP and RUNX2 staining was observed on all 30 kPa hydrogels regardless of sulpho-SANPAH concentration, hydrogel formulation and cell type (Fig. 2d and Supplementary Fig. 7). ASCs were also cultured on 4 kPa hydrogels over a range of sulpho-SANPAH concentrations, and ORO expression was observed in over 30% of ASCs regardless of sulpho-SANPAH concentration (Supplementary Fig. 8). Together, these data indicate that the degree of collagen tethering to the substrate surface had no observable effect on stem cell fate, unlike what has been suggested[15]. Myosin contractility deforms the ECM and is required for matrix-induced differentiation[3,8–10]; thus, to confirm differentiation results, substrate displacements for hydrogels across a range of sulpho-SANPAH concentrations were mapped using TFM (Fig. 2e). Average displacements of beads embedded in hydrogels were independent of sulpho-SANPAH concentration and dependent only on substrate modulus (Fig. 2f), suggesting that for the range of protein–substrate linker concentrations used in this study, the surface density of collagen fibre covalent anchoring points has no impact on how cells deform the underlying substrate.

To determine whether or not differences in rupture lengths, that is, tethering, detected by force spectrograms could be felt by cells on a molecular scale, a fibronectin Förster resonance energy transfer (FRET) sensor[14] was covalently attached to hydrogels in place of collagen. Cell-generated forces unfold the protein thus increasing the distance between paired fluorescent probes, which results in a decrease in the FRET ratio (Supplementary Fig. 9a) that can also be shown by chemical denaturation (Supplementary Fig. 9b,c). Changing sulpho-SANPAH concentration has no statistical effect on the FRET ratio of fibronectin underneath spread ASCs regardless

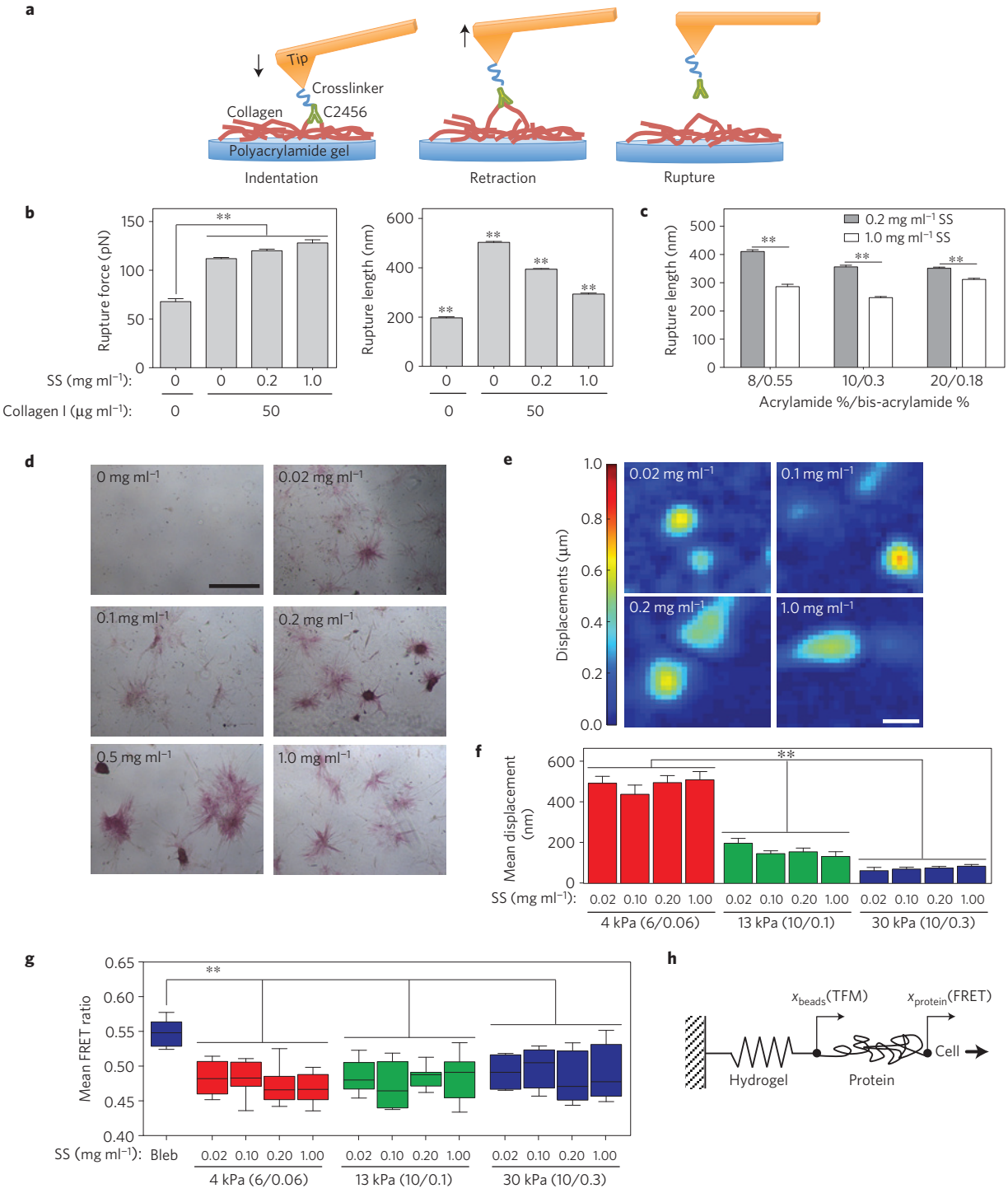

Figure 2 | Influence of protein tethering on ASC differentiation. a, Schematic depicting the interaction between an AFM tip (orange) functionalized with a collagen I antibody (C2456; green) and the hydrogel (blue) functionalized with bound collagen I (red). The black arrow indicates the direction of motion. A rupture event occurs following retraction of the tip from the surface. **b**, Measured rupture force (left) and rupture length (right) for rupture events that occurred on 10/0.3 30 kPa hydrogels activated with the indicated sulpho-SANPAH (SS) and collagen I concentrations ($n=500$; mean ± s.e.m.; $^{**}P<0.0001$). **c**, Rupture length was measured for rupture events that occurred on 30 kPa hydrogels with the indicated monomer-to-crosslinker ratios. Hydrogels were activated with either 0.2 mg ml^{-1} or 1 mg ml^{-1} sulpho-SANPAH. ($n=500$; mean ± s.e.m.; $^{**}P<0.0001$). **d**, Images of ASCs stained for ALP expression on 10/0.3 hydrogels as a function of sulpho-SANPAH concentration after 14 days of culture in normal media. Scale bar, 500 μm. **e**, Displacement maps of embedded fluorescent particles resulting from ASC traction forces on 10/0.3 hydrogels for a range of indicated sulpho-SANPAH concentrations. Scale bar, 50 μm. **f**, Quantification of mean bead displacement for the indicated hydrogel stiffness and composition as well as sulpho-SANPAH (SS) concentration ($n=20$; mean ± s.e.m.; $^{**}P<0.0001$). **g**, Measured fibronectin FRET intensity ratio for ASCs on 4, 14 and 30 kPa hydrogels activated with the indicated concentrations of sulpho-SANPAH ($n=8$; $^{**}P<0.001$). **h**, Proposed model of a cell on a protein-coated substrate attached to a rigid base (glass coverslip) where cell forces are translated through the protein and through the substrate. Deformations of the substrate are measured by TFM and deformations of the protein are measured by FRET.

of hydrogel formulation, whereas perturbing myosin contractility using blebbistatin caused a significant increase in the FRET ratio (Fig. 2g and Supplementary Fig. 9d). Thus, molecular conformational changes in protein caused by ASC traction forces are similar regardless of protein–substrate linker concentration, implying that ASCs deform the surface protein similarly on all sulpho-SANPAH activated hydrogels. On the basis of these findings, we propose that cells deform both the adhesive protein on the hydrogel surface as well as the underlying PA substrate according to the model depicted in Fig. 2h. Cell forces are translated sequentially through the protein layer and the hydrogel. However, our findings suggest that the degree of coupling of the protein to the substrate does not influence substrate deformation and thus differentiation; therefore, it was not depicted in Fig. 2h.

Differentiation occurs in the absence of tethering

To demonstrate that stiffness-induced differentiation is possible in the absence of fibrous protein tethering, RGD, a short cell-adhesive peptide from fibronectin[24], was directly incorporated into the PA backbone by including acrylated polyethylene glycol bound to RGD (acrylated-PEG–RGD) during polymerization rather than by tethering an adhesive protein to the substrate. Three separate hydrogel formulations with 0.1, 0.5 and 2.5 mM RGD yielding the same gel stiffness were made for 4, 13 and 30 kPa substrates using the acrylamide/bis-acrylamide ratios listed above (Fig. 3a). A hydroxycoumarin dye-conjugated acrylated-PEG–RGD confirmed that the peptide was incorporated in a dose-dependent manner (Fig. 3b). SEM images of dried hydrogels show similar pore sizes regardless of the concentration of acrylated-PEG–RGD incorporated within each substrate (Fig. 3c). This ensures that differentiation effects can be attributed to changes in adhesive-peptide density and not porosity. Furthermore, to ensure that the PEG moiety does not act as a tether, individual force spectrograms were obtained from biotin-terminated PEG-coated PA hydrogels and an avidin-functionalized probe. Larger rupture forces and a greater number of rupture events were detected on substrates before blocking with excess avidin in solution (Fig. 3d, left and middle), which indicate that the avidin-functionalized probe was specifically bound to the biotin-coated surface. Rupture lengths before and after blocking were not statistically different (Fig. 3d, right) and were similar to rupture lengths measured on control PA substrates with no surface coating (Fig. 2b, right). In contrast to collagen-coated PA substrates that exhibited significantly greater rupture lengths, the deformations of the PEG moiety are minimal. Thus, PA–PEG–RGD substrates are a valid culture platform absent of protein tethering for the given concentration range and size of PEG tested. ASCs were then cultured for 14 days in normal growth media to determine whether differentiation was possible without tethering over the range of peptide concentrations tested. ASCs underwent osteogenic differentiation on 10/0.3 30 kPa hydrogels independently of RGD concentration (Fig. 3e). Furthermore, osteogenic differentiation was seen in ASCs and MSCs cultured on all 30 kPa hydrogel formulations with 2.5 mM RGD (Fig. 3f and Supplementary Fig. 10). Together, these data suggest that differentiation occurs in the absence of fibrous protein tethering over the range of peptide concentrations tested. Cell-generated substrate displacements were similar to that of collagen-coated hydrogels (Fig. 3g), lending further evidence that matrix-induced differentiation operates through common myosin-based contractile mechanisms given that differentiated cells on these and collagen-coated hydrogels were similar.

Cell spread area on PA and PDMS substrates

To further support the claim that stiffness mediates cell functions generally, we observed the basic behaviour of cell spreading on PA–PEG–RGD hydrogels in the absence of protein tethers. ASC spread area 24 h after seeding scaled with increasing hydrogel stiffness (Supplementary Fig. 11a). This suggests that stiffness is an important physical factor regardless of how adhesive ligands are presented (although dependent on concentration[25]). To determine whether or not this phenomenon is specific to acrylamide-based systems, polydimethylsiloxane (PDMS) substrates were fabricated with base-to-curing ratios of 100:1, 75:1 and 50:1 to modulate stiffness as noted previously[15]. These substrates were not functionalized with adhesive protein. Without covalently attaching or tethering ligands to the surface, cell adhesion and spreading was still possible for all substrates, owing to the well-known fouling properties of PDMS. Furthermore, cell spread area was similar on all substrates (Supplementary Fig. 11b). This observation is in agreement with previous observations that imply stiffness-independent cell spreading on PDMS substrates[15], suggesting that cells may sense similar mechanical cues on the three PDMS formulations.

PDMS mechanical properties on a cell-sensing scale

Owing to a lack of correlation between cell spread area and PDMS base-to-curing ratio, we independently measured PDMS stiffness by atomic force microscopy (AFM) microindentation. The stiffnesses of 50:1 and 100:1 PDMS were found to be 250 and 550 kPa (Supplementary Fig. 12a)—orders of magnitude greater than previously reported[15]. As PDMS has previously been shown to be viscoelastic at higher base-to-curing ratios[26], substrates were instead indented using different indenter geometries and at different indentation speeds. Indenting substrates with two different probes and a wide range of indentation speeds confirmed the viscoelastic behaviour of PDMS (Supplementary Fig. 12b) and suggests that different methods of characterization may account for discrepancies in reported values of PDMS stiffness.

Given the lack of consensus on measuring the mechanical properties of PDMS, it is important to use the most appropriate technique to closely mimic cell–substrate interactions. Cells pull against substrates at 20–120 nm s^{-1}, resulting in deformations that scale inversely with stiffness[17,27] (Fig. 4a). We can match AFM tip- retraction velocity to the pulling velocity and size of focal adhesions. Consequently, we can simulate these dynamically fluctuating pulling events by analysing the retraction curves (as opposed to indentation curves) obtained by AFM where the tip has pulled and deformed the material above the surface (Fig. 4b). The substrate stiffness is determined by fitting the linear region beginning at the contact point with the (undeformed) surface ($F = 0$ pN) to where the force reaches -100 pN (Fig. 4c). PA hydrogels of 1 and 30 kPa demonstrated little variation in stiffness over a range of cell-relevant strains[26] and retraction speeds[17,27]. The stiffnesses of 50:1 and 100:1 PDMS were both significantly higher than the PA hydrogels, and the stiffness of 100:1 PDMS increases 50-fold over the range of retraction velocities tested (Fig. 4d). These data confirm that 100:1 PDMS is highly viscoelastic and 50:1 PDMS is predominantly elastic, but both are stiff over cell-relevant strains in agreement with previous data[26]. Although previous studies have noted lower stiffness values of PDMS for the same cure ratios[15], it is well known that the mechanical properties of PDMS are different at the cellular mechanosensing scale than at the macroscopic scale[28]. At the scale at which a cell mechanosenses[17,27], both 50:1 and 100:1 PDMS substrates are stiffer than 30 kPa PA hydrogels (Fig. 4d). This provides a reasonable explanation as to why cell spreading (Supplementary Fig. 11b) and osteogenic differentiation (Fig. 4e), neither of which changed with cure ratio, were previously reported to be stiffness independent[15]. We note here, however, that it is possible to decrease the effective stiffness of PDMS by fabricating microposts of identical cure ratios but different heights. In ref. 28, it was found that MSC contractility and differentiation towards adipogenic or osteogenic lineages scaled as a function of effective stiffness pillar height. Thus, even

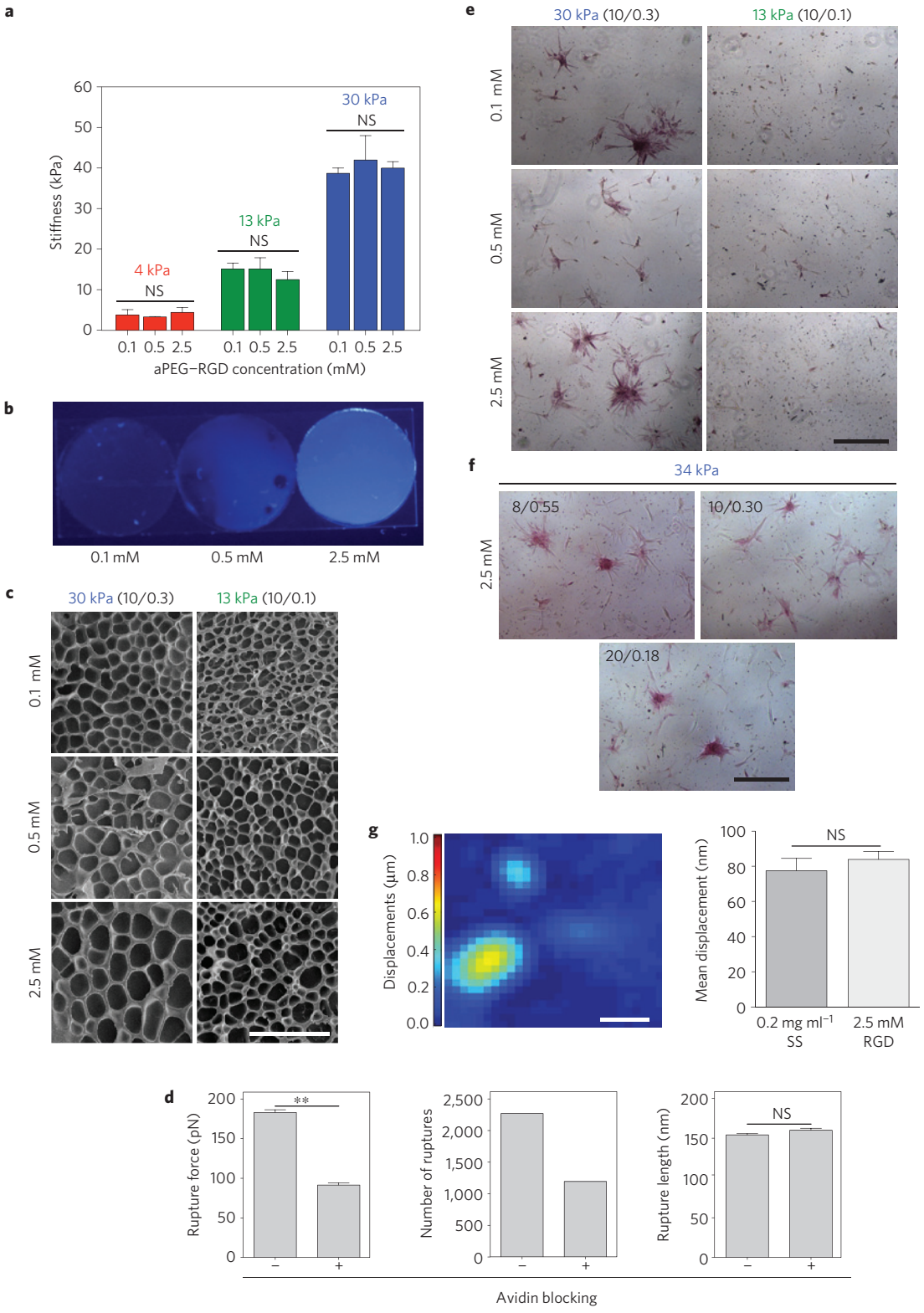

Figure 3 | Direct incorporation of a short adhesive peptide to the PA substrate. a, Elastic modulus measured by AFM (mean ± s.d.; $n=3$; NS, not significant). **b**, aPEG–RGD–dye incorporation is detected under ultraviolet light. **c**, SEM images of PA hydrogels of the indicated stiffness made with varying RGD concentration. Scale bar, 50 μm. **d**, Measured rupture force (left), number of events (middle), and rupture length (right) for rupture events that occurred on 10/0.3 30 kPa hydrogels coated with PEG–biotin ($n=1,000$; mean ± s.e.m.; NS, not significant; $^{**}P<0.0001$). **e**, ALP staining of ASCs on 13 kPa and 30 kPa hydrogels with low, medium and high concentrations of RGD. Scale bar, 500 μm. **f**, ALP staining of ASCs on 30 kPa hydrogels of varying monomer-to-crosslinker ratio and constant high concentration of RGD after 14 days of culture in normal media. Scale bar, 500 μm. **g**, Representative displacement map (left) of embedded fluorescent particles resulting from ASC traction forces on a 30 kPa hydrogel with 2.5 mM RGD. Mean displacement is shown (right) for a collagen-coated hydrogel (0.2 mg ml^{-1} sulpho-SANPAH and 50 μg ml^{-1} collagen I) and a PA–PEG–RGD hydrogel (2.5 mM RGD). ($n=30$; mean ± s.e.m.; NS, not significant; scale bar, 50 μm.)

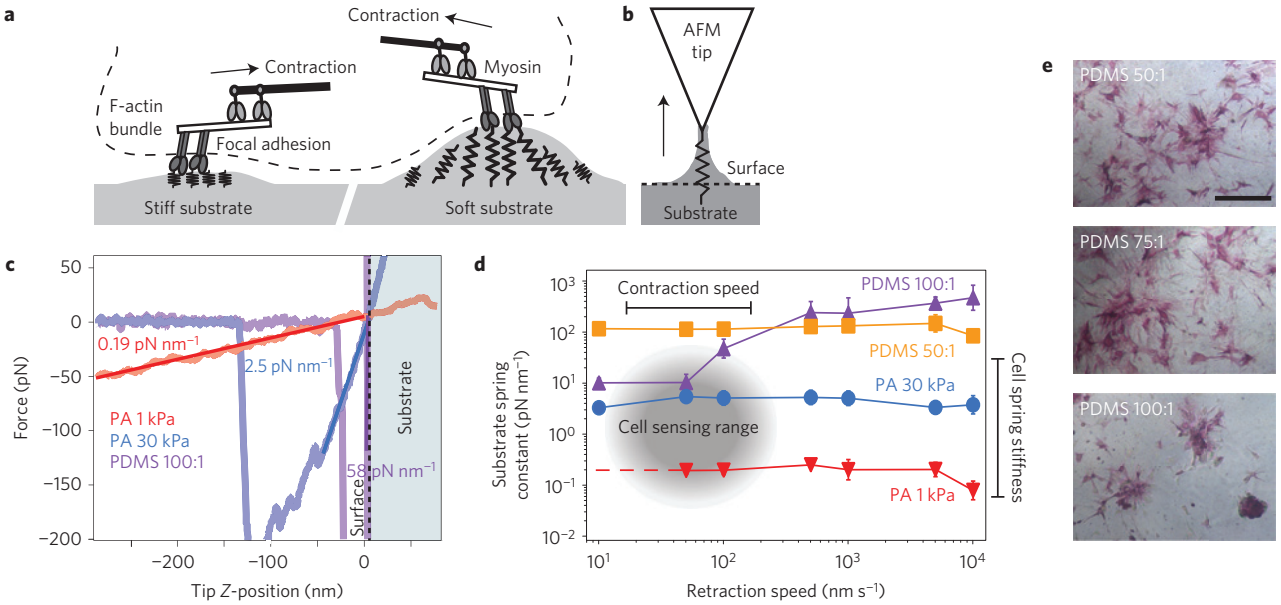

Figure 4 | Cells sense by contracting against their substrates. a, Schematic depicting how cells dynamically deform soft and stiff substrates by pulling (and not pushing) through myosin contractions. Softer substrates are deformed to a greater extent than stiffer substrates. **b**, Schematic depicting the interaction between an AFM tip and the surface of a substrate. The arrow indicates the direction of motion of the tip during retraction. **c**, Representative retraction curves for 1 and 30 kPa PA hydrogels and a 100:1 PDMS substrate. The dashed line indicates the point at which the tip is no longer indenting into the substrate (shaded light blue). Substrate stiffness is calculated by fitting the linear region of the retraction curve starting at the (undeformed) surface. **d**, Substrate spring constant determined by the method depicted in **c** for 1 and 30 kPa PA hydrogels and 50:1 and 100:1 PDMS substrates as a function of AFM tip retraction speed (mean ± s.d.). Cells are sensitive to substrate stiffnesses of 1–100 kPa. Previously measured myosin contraction speeds range from 10–100 nm s^{-1} (grey). **e**, ALP staining of ASCs on PDMS substrates after 7 days of culture in normal media. Scale bar, 500 μm.

in PDMS systems where cure ratio is not directly modulated, effectively modulating stiffness can still yield mechanically driven differentiation.

PDMS substrates do not support protein tethering

To address the possibility of fibrous protein tethering on PDMS, 50:1 PDMS substrates were examined using force spectroscopy. When 50:1 PDMS substrates were pre-incubated in a collagen solution, rupture events with lengths and forces much greater than that of PA substrates were detected (Fig. 5a), confirming that collagen nonspecifically adsorbs to PDMS. Attempting to functionalize PDMS with sulpho-SANPAH before collagen incubation[15] did not alter the rupture force (Fig. 5b). However, the rupture length markedly increased from 450 nm to 1.5 μm, which is larger than cell deformations on stiff PA substrates (Figs 2g and 5a). This observation is opposite to what was seen with PA; treating PA with sulpho-SANPAH increases fibrous- collagen tethering to PA, consequently decreasing the rupture length (Fig. 2b).

The increased rupture lengths seen in PDMS may be attributed to the formation of long chains of collagen forming on the PDMS surface as collagen contains many primary amines for sulpho-SANPAH to crosslink, whereas PDMS is void of amines (Supplementary Fig. 13a, left). In this hypothesis, sulpho-SANPAH is not directly coupled to the PDMS surface, but rather only to collagen chains. To test this hypothesis, substrates were functionalized with sulpho-SANPAH before incubation in NH_2–PEG–biotin, which has only one free primary amine (Supplementary Fig. 13a, right). Rupture lengths and forces obtained from force spectrograms using avidin tips were similar on biotin-coated substrates functionalized with and without sulpho-SANPAH (Fig. 5a).

To further confirm that sulpho-SANPAH does not react with PDMS, amines were covalently bound to PDMS substrate surfaces using the chemistry outlined in Supplementary Fig. 13b. At least one rupture event was detected in more than 90% of the force spectrograms obtained from biotin-coated samples. In contrast, rupture events were detected in only 30% of the force spectrograms obtained from biotin-coated but not amine-functionalized PDMS samples independently of sulpho-SANPAH (Fig. 5b). Thus, it is clear that the sulpho-succinimidyl group requires amines to form a covalent bond. Regardless of ultraviolet treatment, PDMS surfaces do not display free amines, and thus protein cannot be covalently bound to the surface through sulpho-SANPAH. Previous efforts do not seem to have amine-functionalized PDMS (ref. 15), and thus it is difficult to attribute fibrous- protein tethering on PDMS to cell spreading and differentiation. These results, in conjunction with cure ratio-independent stem cell spreading (Supplementary Fig. 11b) and differentiation (Fig. 4e), emphasize the shortcomings of PDMS as a model system to investigate stiffness-dependent behaviour over a relevant cell-sensing range[28]. Elastic two-dimensional hydrogel systems with controlled stiffness such as PA, PEG (ref. 29), hyaluronic acid[30,31] and alginate[32] are better suited to investigate these cell behaviours.

Summary

The commonly used PA hydrogel system is easily tuned to modulate substrate porosity, and in combination with different concentrations of sulpho-SANPAH, provides a platform to investigate how substrate stiffness, porosity and ligand tethering affect stem cell fate. The data presented here provide direct evidence that the mechanical feedback provided by hydrogel deformations on planar matrices regulates osteogenic and adipogenic differentiation of ASCs and MSCs independently of protein tethering and substrate porosity. Furthermore, these data indicate that substrates have fibrous-protein tethers as previously suggested[15]; however, these tethers are not essential for the osteogenic and adipogenic differentiation of ASCs and MSCs. This work further highlights the importance of bulk matrix stiffness as the main mechanical regulator of stem cell differentiation.

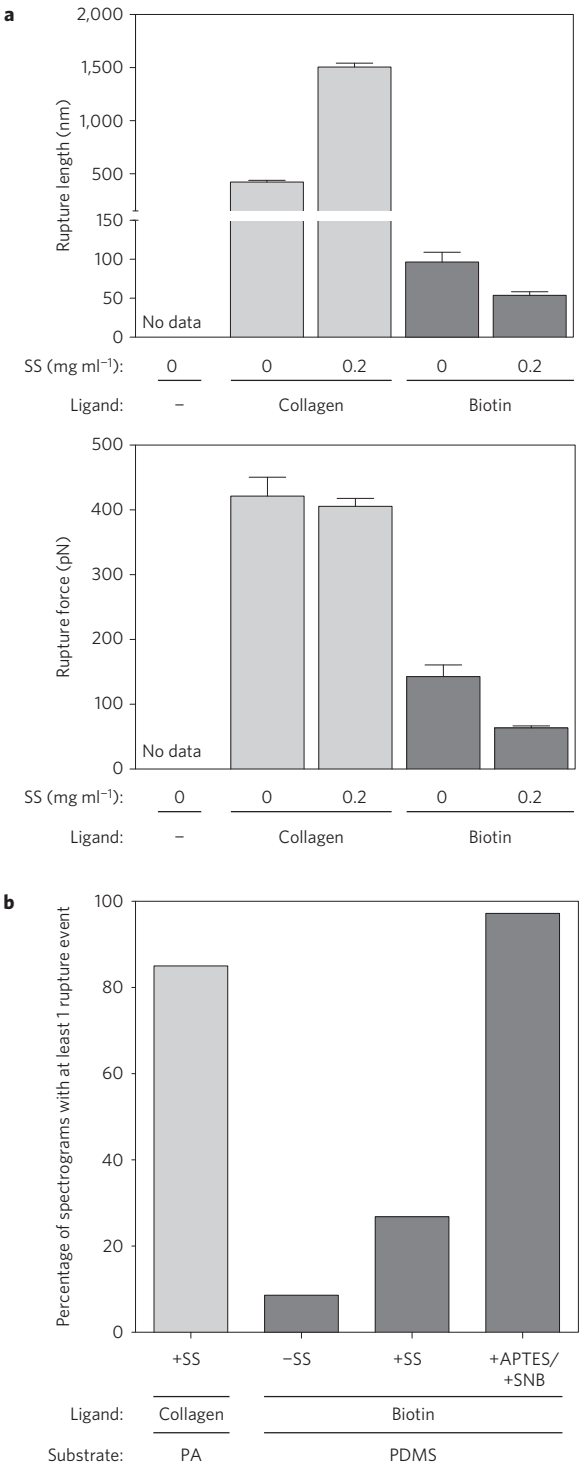

Figure 5 | Atomic force spectrography analysis of ligand-coated PDMS substrates. a, Measured rupture length (top) and rupture force (bottom) for rupture events detected on 50:1 PDMS substrates activated with the indicated sulpho-SANPAH (SS) and collagen or NH_2–PEG–biotin concentrations (mean ± s.e.m.). No data indicates that no rupture events were detected. **b**, Percentage of spectrograms with at least one rupture event on PA and PDMS substrates activated with the linkers and ligands shown.

Methods

PA gels. Glass coverslips were functionalized using 3-(trimethoxysilyl)propyl methacrylate to facilitate covalent attachment of hydrogel substrates to glass. A polymer solution containing acrylamide monomers, crosslinker *N*,*N* methylene-bis-acrylamide, ammonium persulphate and *N*,*N*,*N*′,*N*′-tetramethylethylenediamine (TEMED) was prepared. The polymerizing solution was sandwiched between a functionalized coverslip and a dichlorodimethylsilane-treated slide to ensure easy detachment of hydrogels. The ratio of acrylamide%/bis-acrylamide% was varied to control hydrogel stiffness and porosity. To allow for cell adhesion and fibrous- protein tethering, substrates were incubated in 0.02, 0.1, 0.2, 0.5 or 1 mg ml^{-1} *N*-sulphosuccinimidyl-6-(4′-azido-2′-nitrophenylamino) hexanoate (sulpho-SANPAH), activated with ultraviolet light, washed, and then incubated in collagen overnight. For AFM experiments, 0.5 mg ml^{-1} amine–PEG3400–biotin was used instead of collagen. Coated hydrogels were ultraviolet sterilized before use in cell culture.

PA–PEG–RGD gels. PA–PEG–RGD hydrogels were fabricated by incorporating 0.1 mM, 0.5 mM or 2.5 mM acrylated-PEG3400–GRGD-amide (aPEG–RGD) into the polymerizing solution described above. To visualize RGD concentration differences, a fluorescent hydroxycoumarin dye was conjugated to the peptide.

PDMS substrates. PDMS was mixed at various elastomer base/curing agent ratios (50:1, 75:1, 90:1, 100:1), thoroughly mixed, and degassed under vacuum before pouring directly into multi-well plates or onto coverslips and baked overnight. In certain instances, substrates were functionalized with sulpho-SANPAH and ligand (Supplementary Information and Supplementary Fig. 13a). For covalent attachment of moieties to the surface, PDMS substrates were treated with ultraviolet/ozone following an incubation under vacuum in the presence of (3-aminopropyl)triethoxysilane. Surfaces were then incubated in sulpho-NHS–biotin (Supplementary Fig. 13b).

SEM. PA and PA–PEG–RGD solutions were polymerized. Hydrogels were swelled in water overnight, flash frozen, then lyophilized overnight. Lyophilized samples were sputter coated with iridium.

DNA gel electrophoresis. DNA ladders were run through PA electrophoresis gels in TAE buffer with ethidium bromide at 30 V for 14 h. DNA fragment lengths were converted to radius of gyration as described elsewhere[22].

Stem cell culture. Human ASCs were isolated from freshly aspirated human subcutaneous adipose tissue according to the method described elsewhere[33]. Commercially available MSCs were purchased. MSCs and ASCs were cultured in Dulbecco's modified eagle medium with fetal bovine serum and antibiotics. For differentiation experiments, MSCs and ASCs were seeded on PA and PDMS substrates at a density of 1,000 cells cm^{-2} and on PA–PEG–RGD gels at a density of 2,000 cells cm^{-2}. See Supplementary Information for inductive media formulations.

Immunofluorescence. Cells were fixed, permeabilized and then stained with rhodamine phalloidin and Hoechst. For osteogenic differentiation studies, cells were stained with RUNX2. To quantify RUNX2 expression, CellProfiler[34] (Broad Institute) was used to measure cytoplasmic and nuclear fluorescent intensities using the nuclei and cell outlines as masks to define these regions of interest in the RUNX2 fluorescent channel.

Differentiation assays. ASCs and MSCs were stained for ALP and ORO as per manufacturer protocols. See Supplementary Information for additional methods.

AFM. To determine the mechanical properties of PA hydrogels by indentation and to quantify protein tethering by force spectroscopy, a MFP-3D-Bio atomic force microscope was used. Chromium/gold-coated, silicone nitride cantilevers with pyramid-shaped tips with ~50 pN nm^{-1} nominal spring constants were used for both methods. Samples were indented at a velocity of 2 μm s^{-1} until a trigger of 2 nN was detected using. All AFM data were analysed using custom-written code in Igor Pro to determine Young's modulus as previously described[35]. PDMS substrates were indented with the same cantilevers mentioned above. In addition, a cantilever with a 45-μm-diameter polystyrene bead tip with 0.03 N m^{-1} nominal spring constant was used. For retraction experiments, samples were indented with approach and retraction velocities ranging from 1 nm s^{-1} to 10 μm s^{-1}. The substrate spring constants were determined by fitting the linear portion of the retraction curve starting at the undeformed surface.

For force spectroscopy, cantilevers were functionalized (Fig. 3a) with an anti-collagen type I antibody, or avidin using a previously established method[36,37]. Briefly, cantilevers were cleaned with chloroform and immersed in ethanolamine-HCl in dimethylsulphoxide. Tips were incubated in bis(sulphosuccinimidyl)suberate, rinsed, and then immersed either in an antibody or avidin solution to crosslink the protein to the tip. Force curves were taken in a regular 10 × 10 array of points spaced ~10 μm apart. To promote binding of the antibody to collagen or avidin to biotin, a dwell time of 1 s was added between approach and retraction cycles. Force curves were converted to force versus tip *Z*-position curves (Supplementary Fig. 6a) and then analysed for

rupture events using a previously described algorithm[38]; rupture lengths and forces were determined.

Traction force microscopy. Traction force microscopy was performed as previously described[23]. Briefly, fluorescent 0.2 μm microspheres were added to the pre-polymer solution. Substrates were functionalized and treated as described above. The microspheres underneath selected live cells were imaged with a confocal imaging system. Cells were released with trypsin and the same confocal stacks were acquired. Bead displacements were determined using a particle image velocimetry MATLAB script.

FRET. Concentrated fibronectin was denatured in guanidine hydrochloride and dual-labelled with donor and acceptor fluorophores, as previously described[13]. Denatured fibronectin was incubated with a molar excess of Alexa Fluor 546 C5 maleimide and subsequently buffer exchanged into sodium bicarbonate. The single-labelled fibronectin was then incubated with a molar excess of Alexa Fluor 488 succinimidyl ester. Unreacted donor fluorophores were removed using a spin desalting column. The emission spectrum of the dual-labelled fibronectin was characterized in varying concentrations of denaturant by fluorescence spectroscopy. The resulting emission spectrum was measured from 510 to 700 nm (Supplementary Fig. 9b) and the ratio of the maximum acceptor emission (~570 nm) to the maximum donor emission (~520 nm) was determined at each concentration of GdnHCl (Supplementary Fig. 9c). Images of the dual-labelled fibronectin were acquired using a confocal microscope and analysed using a custom MATLAB script, as previously described[14]. The mean FRET ratio within the selected regions was calculated for each cell and then averaged over all of the cells in each condition ($n = 16$ cells per condition; Fig. 2g).

See Supplementary Information for additional methods.

Received 9 January 2014; accepted 4 July 2014; published online 10 August 2014

References

1. Pelham, R. J. Jr & Wang, Y. Cell locomotion and focal adhesions are regulated by substrate flexibility. *Proc. Natl Acad. Sci. USA* **94,** 13661–13665 (1997).
2. Gilbert, P. M. *et al.* Substrate elasticity regulates skeletal muscle stem cell self-renewal in culture. *Science* **329,** 1078–1081 (2010).
3. Engler, A. J., Sen, S., Sweeney, H. L. & Discher, D. E. Matrix elasticity directs stem cell lineage specification. *Cell* **126,** 677–689 (2006).
4. Choi, Y. S., Vincent, L. G., Lee, A. R., Dobke, M. K. & Engler, A. J. Mechanical derivation of functional myotubes from adipose-derived stem cells. *Biomaterials* **33,** 2482–2491 (2012).
5. Saha, K. *et al.* Substrate modulus directs neural stem cell behavior. *Biophys. J.* **95,** 4426–4438 (2008).
6. Rowlands, A. S., George, P. A. & Cooper-White, J. J. Directing osteogenic and myogenic differentiation of MSCs: Interplay of stiffness and adhesive ligand presentation. *Am. J. Physiol. Cell Physiol.* **295,** C1037–C1044 (2008).
7. Engler, A. J., Sen, S., Sweeney, H. L. & Discher, D. E. Matrix elasticity directs stem cell lineage specification. *Cell* **126,** 677–689 (2006).
8. McBeath, R., Pirone, D. M., Nelson, C. M., Bhadriraju, K. & Chen, C. S. Cell shape, cytoskeletal tension, and RhoA regulate stem cell lineage commitment. *Dev. Cell* **6,** 483–495 (2004).
9. Dupont, S. *et al.* Role of YAP/TAZ in mechanotransduction. *Nature* **474,** 179–183 (2011).
10. Kilian, K. A., Bugarija, B., Lahn, B. T. & Mrksich, M. Geometric cues for directing the differentiation of mesenchymal stem cells. *Proc. Natl Acad. Sci. USA* **107,** 4872–4877 (2010).
11. Huebsch, N. *et al.* Harnessing traction-mediated manipulation of the cell/matrix interface to control stem-cell fate. *Nature Mater.* **9,** 518–526 (2010).
12. Khetan, S. *et al.* Degradation-mediated cellular traction directs stem cell fate in covalently crosslinked three-dimensional hydrogels. *Nature Mater.* **12,** 458–465 (2013).
13. Baneyx, G., Baugh, L. & Vogel, V. Fibronectin extension and unfolding within cell matrix fibrils controlled by cytoskeletal tension. *Proc. Natl Acad. Sci. USA* **99,** 5139–5143 (2002).
14. Smith, M. L. *et al.* Force-induced unfolding of fibronectin in the extracellular matrix of living cells. *PLoS Biol.* **5,** e268 (2007).
15. Trappmann, B. *et al.* Extracellular-matrix tethering regulates stem-cell fate. *Nature Mater.* **11,** 642–649 (2012).
16. Rossman, J. S. & Dym, C. L. *Introduction to Engineering Mechanics: A Continuum Approach* (CRC Press, 2008).
17. Plotnikov, S. V., Pasapera, A. M., Sabass, B. & Waterman, C. M. Force fluctuations within focal adhesions mediate ECM-rigidity sensing to guide directed cell migration. *Cell* **151,** 1513–1527 (2012).
18. Holle, A. W. *et al. In situ* mechanotransduction via vinculin regulates stem cell differentiation. *Stem Cells* **31,** 2467–2477 (2013).
19. Lutolf, M. P., Gilbert, P. M. & Blau, H. M. Designing materials to direct stem-cell fate. *Nature* **462,** 433–441 (2009).
20. Guilak, F. *et al.* Control of stem cell fate by physical interactions with the extracellular matrix. *Cell Stem Cell* **5,** 17–26 (2009).
21. Discher, D. E., Mooney, D. J. & Zandstra, P. W. Growth factors, matrices, and forces combine and control stem cells. *Science* **324,** 1673–1677 (2009).
22. Stellwagen, N. C. Apparent pore size of polyacrylamide gels: Comparison of gels cast and run in tris-acetate-EDTA and tris-borate-EDTA buffers. *Electrophoresis* **19,** 1542–1547 (1998).
23. Del Alamo, J. C. *et al.* Three-dimensional quantification of cellular traction forces and mechanosensing of thin substrata by fourier traction force microscopy. *PLoS ONE* **8,** e69850 (2013).
24. Ruoslahti, E. & Pierschbacher, M. D. New perspectives in cell adhesion: RGD and integrins. *Science* **238,** 491–497 (1987).
25. Engler, A. *et al.* Substrate compliance versus ligand density in cell on gel responses. *Biophys. J.* **86,** 617–628 (2004).
26. Murrell, M., Kamm, R. & Matsudaira, P. Substrate viscosity enhances correlation in epithelial sheet movement. *Biophys. J.* **101,** 297–306 (2011).
27. Bangasser, B. L., Rosenfeld, S. S. & Odde, D. J. Determinants of maximal force transmission in a motor-clutch model of cell traction in a compliant microenvironment. *Biophys. J.* **105,** 581–592 (2013).
28. Fu, J. *et al.* Mechanical regulation of cell function with geometrically modulated elastomeric substrates. *Nature Methods* **7,** 733–736 (2010).
29. Khatiwala, C. B., Peyton, S. R., Metzke, M. & Putnam, A. J. The regulation of osteogenesis by ECM rigidity in MC3T3-E1 cells requires MAPK activation. *J. Cell. Physiol.* **211,** 661–672 (2007).
30. Young, J. L. & Engler, A. J. Hydrogels with time-dependent material properties enhance cardiomyocyte differentiation *in vitro*. *Biomaterials* **32,** 1002–1009 (2011).
31. Chopra, A. *et al.* Reprogramming cardiomyocyte mechanosensing by crosstalk between integrins and hyaluronic acid receptors. *J. Biomech.* **45,** 824–831 (2012).
32. Kong, H. J., Polte, T. R., Alsberg, E. & Mooney, D. J. FRET measurements of cell-traction forces and nano-scale clustering of adhesion ligands varied by substrate stiffness. *Proc. Natl Acad. Sci. USA* **102,** 4300–4305 (2005).
33. Choi, Y. S. *et al.* The alignment and fusion assembly of adipose-derived stem cells on mechanically patterned matrices. *Biomaterials* **33,** 6943–6951 (2012).
34. Carpenter, A. E. *et al.* CellProfiler: Image analysis software for identifying and quantifying cell phenotypes. *Genome Biol.* **7,** R100 (2006).
35. Kaushik, G. *et al.* Measuring passive myocardial stiffness in *Drosophila melanogaster* to investigate diastolic dysfunction. *J. Cell. Mol. Med.* **16,** 1656–1662 (2012).
36. Bonanni, B. *et al.* Single molecule recognition between cytochrome C 551 and gold-immobilized azurin by force spectroscopy. *Biophys. J.* **89,** 2783–2791 (2005).
37. Chirasatitsin, S. & Engler, A. J. Detecting cell-adhesive sites in extracellular matrix using force spectroscopy mapping. *J. Phys. Condens. Matter* **22,** 194102 (2010).
38. Fuhrmann, A., Anselmetti, D., Ros, R., Getfert, S. & Reimann, P. Refined procedure of evaluating experimental single-molecule force spectroscopy data. *Phys. Rev. E* **77,** 031912 (2008).

Acknowledgements

The authors thank M. Joens, J. Kasuboski and J. Fitzpatrick at the Waitt Advanced Biophotonics Center at the Salk Institute (supported by NCI P30 Cancer Center Support Grant CA014195-40 and NINDS P30 Neuroscience Center Core Grant NS072031-03A1 and by the W. M. Keck Foundation) for technical assistance with microscopy, and W. Murphy (University of Wisconsin), T. McDevitt (Georgia Tech) and J. C. del Alamo (UC San Diego) for helpful conversations. The National Institutes of Health (DP02OD006460 to A.J.E.), the Human Frontiers Science Program (RGY0064/2010 to A.J.E.), the National Science Foundation Graduate Research Fellowship Program (to J.H.W., L.G.V. and H.T-W.), the Siebel Scholars Program, and the Achievement Rewards for College Scientists (to L.G.V.) supported this work.

Author contributions

All authors contributed to the design of experiments. Y.S.C., K.C.H. and S.C. characterized the hydrogel substrates. H.T-W. characterized and performed experiments with the FRET probe. J.H.W., L.G.V. and A.F. conducted all other experiments and performed the data analysis. J.H.W., L.G.V. and A.J.E. wrote the manuscript.

Additional information

Supplementary information is available in the online version of the paper. Reprints and permissions information is available online at www.nature.com/reprints. Correspondence and requests for materials should be addressed to A.J.E.

Competing financial interests

The authors declare no competing financial interests.